NASA TECHNICAL NOTE

NASA TN D-7047

NASA TN D-7047

EXPERIMENTAL AERODYNAMIC PERFORMANCE CHARACTERISTICS OF A ROTOR ENTRY VEHICLE CONFIGURATION

II – Transonic

by Alan D. Levin and Ronald C. Smith

Ames Research Center
Moffett Field, Calif. 94035

NATIONAL AERONAUTICS AND SPACE ADMINISTRATION • WASHINGTON, D. C. • FEBRUARY 1971

1. Report No.	2. Government Accession No.	3. Recipient's Catalog No.
NASA TN D-7047		

4. Title and Subtitle
EXPERIMENTAL AERODYNAMIC PERFORMANCE CHARACTERISTICS OF A ROTOR ENTRY VEHICLE CONFIGURATION. II – TRANSONIC

5. Report Date
February 1971

6. Performing Organization Code

7. Author(s)
Alan D. Levin and Ronald C. Smith

8. Performing Organization Report No.
A-3710

10. Work Unit No.
124-07-11-11-00-21

9. Performing Organization Name and Address
NASA Ames Research Center
Moffett Field, Calif., 94035

11. Contract or Grant No.

13. Type of Report and Period Covered
Technical Note

12. Sponsoring Agency Name and Address
National Aeronautics and Space Administration
Washington, D. C., 20546

14. Sponsoring Agency Code

15. Supplementary Notes

16. Abstract

Wind-tunnel tests were conducted to determine the aerodynamic performance characteristics of an unpowered rotor entry vehicle configuration at Mach numbers from 0.91 to 1.11. Blade collective pitch angle was varied for model angles of attack from 15° to 90°. The effectiveness of cyclic pitch controls at 15° and 25° angle of attack was also tested. Rotor blade configurations having double wedge and modified ellipse profiles were tested in combination with a 15-inch diameter capsule forebody. The ellipse profile was tested for rotor diameters of 45 and 60 inches.

It was found that neither blade-section shape nor Mach number had significant effect on the aerodynamic characteristics. The rotor produced large positive pitching moments at low and intermediate angles of attack which could not be trimmed with the range of cyclic pitch controls available. Moderate rolling moments were produced by the rotor which could be trimmed with the longitudinal cyclic pitch control. The maximum lift-drag ratio was about 0.75 for the short blade configurations and nearly 1.0 for the long blade configuration.

17. Key Words (Suggested by Author(s))	18. Distribution Statement
Entry Vehicles **Rotor Performance** **Rotor Aerodynamics** **Transonic** **Autorating Characteristics**	Unclassified – Unlimited

19. Security Classif. (of this report)	20. Security Classif. (of this page)	21. No. of Pages	22. Price*
Unclassified	Unclassified	44	$3.00

*For sale by the National Technical Information Service, Springfield, Virginia 22151

NOTATION

The body-axes, force and moment coefficients, and angles used are shown in figure 1.

b number of blades

c blade chord

C_D drag coefficient, $\frac{\text{drag}}{q_\infty S}$

C_L lift coefficient, $\frac{\text{lift}}{q_\infty S}$

C_l body axis rolling-moment coefficient, $\frac{\text{rolling moment}}{q_\infty Sd}$

C_m pitching-moment coefficient, $\frac{\text{pitching moment}}{q_\infty Sd}$

C_N normal-force coefficient, $\frac{\text{normal coefficient}}{q_\infty S}$

C_X axial-force coefficient, $\frac{\text{axial force}}{q_\infty S}$

C_Y side-force coefficient, $\frac{\text{side force}}{q_\infty S}$

d capsule diameter

$\frac{L}{D}$ lift-drag ratio

M_∞ free-stream Mach number

q_∞ free-stream dynamic pressure

R rotor-blade radius measured normal to the axis of rotation with the blades in the fully open ($\beta = 0°$) position

R_{LE} blade-section leading-edge radius

S capsule reference area, $\frac{\pi d^2}{4}$

V_∞ free-stream velocity

$\frac{\Omega R}{V_\infty}$	dimensionless tip speed
α	angle of attack, angle between relative wind and a plane normal to the shaft axis
β	flapping angle
$\theta\ (\psi)$	blade pitch angle, $\theta_O - \theta_1 \sin \psi + \theta_2 \cos \psi$
θ_O	collective pitch angle
θ_1	longitudinal cyclic pitch (sine feathering amplitude)
θ_2	lateral cyclic pitch (cosine feathering amplitude)
σ	rotor solidity, $\frac{bc}{\pi R}$
ψ	blade azimuth angle
Ω	rotor angular velocity

EXPERIMENTAL AERODYNAMIC PERFORMANCE CHARACTERISTICS OF A ROTOR ENTRY VEHICLE CONFIGURATION

II - TRANSONIC

Alan D. Levin and Ronald C. Smith

Ames Research Center

SUMMARY

Wind-tunnel tests were conducted to determine the aerodynamic performance characteristics of an unpowered rotor entry vehicle configuration at Mach numbers from 0.91 to 1.11. Blade collective pitch angle was varied for model angles of attack from 15° to 90°. The effectiveness of cyclic pitch controls at 15° and 25° angle of attack was also tested. Rotor blade configurations having double wedge and modified ellipse profiles were tested in combination with a 15-inch-diameter capsule forebody. The ellipse profile was tested for rotor diameters of 45 and 60 inches.

It was found that neither blade-section shape nor Mach number had significant effect on the aerodynamic characteristics. The rotor produced large positive pitching moments at low and intermediate angles of attack which could not be trimmed with the range of cyclic pitch controls available. Moderate rolling moments were produced by the rotor which could be trimmed with the longitudinal cyclic pitch control. The maximum lift-drag ratio was about 0.75 for the short blade configurations and nearly 1.0 for the long blade configuration.

INTRODUCTION

As the recovery of instrumented and manned space capsules becomes more frequent, the need for a recovery system that can provide a safe landing almost anywhere and in adverse weather becomes more urgent. While parachutes, paragliders, and lifting bodies can perform certain missions, none of these recovery systems has the operational flexibility needed to perform a large variety of recovery missions.

One system that appears to possess the desired capabilities is the deployable autorotating rotor. Specifically, the rotor offers the capability of (1) zero speed touchdown; (2) touchdown at an unprepared landing site; and (3) aerodynamic force modulation without changes in the vehicle's attitude. The idea of using a rotor for lift and retardation during recovery from orbit is not new and has been investigated and reported by various authors (see refs. 1-5).

The investigation reported herein is part of a program designed to determine the feasibility of using an autorotating rotor for lift and drag modulation from orbital speed to touchdown. An analytical study has been made to estimate the aerodynamic characteristics of a rotor entry vehicle (REV) configuration and to determine its performance as an entry vehicle. This work has been

reported in reference 6. The entry performance study indicated that the REV could provide substantial range capability if the aerodynamic heating of the rotor blades would not severely restrict the flight envelope. In order to establish the limits on velocity and altitude imposed by blade heating, experiments were made on a small REV model in the Ames 1-foot shock tunnel to measure blade heating rates (ref. 7). The results agree favorably with heating estimates for near-axial flight (flight nearly parallel to rotor axis) and indicate that the rotor can be used for retardation during the entire entry. Heating rates of the blade leading edge measured in glide flight were not valid because of the small size of the model. Heating rates estimated for the leading edge indicate that the rotor can be utilized in glide flight (15° to 25° angle of attack) at speeds below about 16,000 feet per second (200,000 ft altitude) if the blade is radiation-cooled and has a ceramic coating capable of withstanding 3700° F. The study reported in reference 6 indicated that delaying glide flight until a speed of 16,000 feet per second is reached would reduce lateral range from 650 statute miles (glide flight from orbit) to about 500 statute miles.

Unfortunately, all work on rotor systems to date was either theoretical or limited to tests at near-axial attitudes for high forward speeds. Hence, very little was known about the aerodynamic and operating characteristics (rotational speed versus blade pitch) of rotors in high speed glide flight.

The objectives of the experimental test programs, of which this report is a part, are to provide experimental rotor operating (RPM vs blade pitch) and aerodynamic characteristics to substantiate the entry performance of an REV as well as to add substantially to the knowledge of high speed unpowered rotors. Accordingly, a wind-tunnel model of an REV configuration was built and successfully tested at Mach numbers up to 3.5 at angles of attack from 15° to 90°.

This report is the second of a three-part series covering the three speed regimes tested. Parts I and III cover, respectively, the subsonic and supersonic speed regimes. Results of the subsonic tests are reported in reference 8. Table 1 indicates the scope of the experimental investigation to determine the aerodynamic characteristics of the body-rotor configuration.

MODEL DESCRIPTION

The rotor entry vehicle model tested is a four-bladed rotor mounted on a capsule body. The mechanical design and fabrication were performed by the Kaman Aircraft Corporation according to general specifications provided by NASA ARC. Detailed drawings of the model are shown in figure 2. Figure 3 is a photograph of the model mounted in the Langley Transonic Dynamics Wind Tunnel.

Rotor

The rotor blades have variable collective pitch and cyclic pitch and were allowed to flap about offset flapping hinges within predetermined limits; however, they do not have lead-lag freedom. A conventional swashplate was provided for remotely changing both the collective and cyclic pitch either independently or in combination. The total range of collective pitch travel is ±90° but only a 40° range is available through the use of the remote control system. The blades could be attached at

15° increments which allowed the entire collective pitch range to be tested. Both the lateral (cosine feathering) and longitudinal (sine feathering) cyclic pitch amplitudes had a range of ±10°. The design operating tip speed is 1100 ft/sec. A detailed description of the model, control system features, and strength requirements can be found in reference 9.

Blades

Two different blade airfoil sections, a modified ellipse and a double wedge, were tested and are illustrated in figure 4. Blades having the modified ellipse section were tested in two blade lengths which gave rotor diameters of 45 and 60 inches corresponding to solidities of 20 and 15 percent, respectively. The double-wedge section was used only with the smaller rotor diameter. The maximum thickness-to-chord ratio is 0.20. The rotor blades are untwisted and have a rectangular planform. The rotor blades were fabricated of a fiberglass epoxy laminate with most of the fibers oriented in the spanwise (radial) direction, giving the blades an extremely high strength to weight ratio in the radial direction.

Body

The capsule body is a typical blunt entry vehicle shape consisting of a body of revolution about the rotor axis. See figure 2. The maximum diameter of the body is 15 inches, which gives rotor to capsule diameter ratios of 3 and 4 for the 45- and 60-inch-diameter rotors, respectively.

Model Mounting Details

In order to cover the angle-of-attack range from 0° to 90°, three different model mounting arrangements were necessary. In all cases the balance centerline was coincident with the rotor axis as shown in figure 5. For the angles of attack from 0° to 25° (fig. 5(a)), the model and balance were mounted on a 90° elbow attached to the model support sting. In the range from 35° to 65° (fig. 5(b)) the model and balance were mounted on a 30° bent adapter attached to the sting. In the range from 65° to 90° (fig. 5(c)) the model and balance were mounted in line with the sting. For the angles of attack from 35° to 90° the wind-tunnel support system necessitated mounting the model upside down. For this range of angles of attack the model lift was positive in the downward direction.

Flapping stop- For the angles of attack from 0° to 25° a flapping stop (fig. 2(a)) was mounted on the rotor hub to prevent large flapping excursions of the rotor blades when the tunnel was started and when conditions that cause flapping instability occurred during the tests. This stop held flapping to 20°. When the model was mounted in the 35° to 65° attitude, a flapping stop was also required to prevent the rotor blades from striking the support sting. This stop allowed up to 45° of flapping freedom. For tests in the axial configuration, the flapping stop was removed.

Blade cager (axial mounting only)- A blade caging arrangement (fig. 6) held the blades in a stowed position along the support sting during the tunnel starting operation. The cager could be used only when the model was mounted in the axial ($\alpha = 90°$) configuration. After data were taken the rotor could be stopped and re-caged before the tunnel was shut down. The caging mechanism could be remotely controlled.

INSTRUMENTATION AND TEST PROCEDURE

Instrumentation

The model forces were measured by means of a 1.75-inch 6-component internal strain gage balance. Rotor RPM was obtained from two magnetic pickups mounted on the stationary swashplate inside the model. The magnetic pickups are energized by the passage of teeth on the rotating swashplate producing an a.c. output at the tooth-passing frequency. A gap left by the omission of one tooth produces a gap in the harmonic output of each of the magnetic pickups. These gaps in the outputs when viewed simultaneously on a dual-beam oscilloscope allowed determination of the direction of rotation.

Test Procedure

When the tunnel was started with the model in the axial configuration ($\alpha = 90°$), the blades were stowed along the sting and held by the blade cager. After test conditions were reached in the tunnel, the cager was opened and the rotor to allow deployment of the rotor. Both collective pitch and cyclic pitch were used to initiate the deployment which simulated deployment during the recovery process. Before the tunnel was shut down, the blade pitch was set at zero and the rotor was restowed. Under these conditions the rotation stops and the flow forces the blades back along the sting. Finally, the blades were clamped in place by closing the cager. This procedure minimized the possibility of dan ging the rotor during the tunnel shutdown operations. At low and intermediate angles of attack, rotor rotation was initiated at a free-stream dynamic pressure of about 50 psf by use of the collective pitch control.

In the glide attitude ($\alpha = 15°$ to $25°$) it was found to be "unsafe" to operate the rotor at angles of attack less than 15° because of flapping instability. This instability occurs when there is insufficient centrifugal force to generate the required moment about the flapping hinge to balance the aerodynamic moment. The resulting flapping excursions can easily cause blade failure by repeated contact of the blade grip with the flapping stop.

The investigation was conducted by parametrically varying the blade pitch angle at fixed conditions of angle of attack and free-stream Mach number. During the test operations only collective pitch and either longitudinal (sine feathering amplitude) or lateral (cosine feathering amplitude) cyclic pitch were varied. When cyclic pitch was varied, the collective pitch angle was held constant. Throughout the tests the model was maintained at zero sideslip angle. Rotor rotation was always clockwise when viewed from the top.

WIND TUNNEL, TEST CONDITIONS, AND DATA ACCURACY

The tests were conducted in the Langley Transonic Dynamics Wind Tunnel which operates continuously from Mach number 0 to 1.20 at maximum stagnation pressures ranging from atmospheric at low speeds to less than 300 psf at maximum speed. The test section is slotted and about 16 feet square filleted corners.

The tests were conducted at total pressures ranging from 170 to 250 psf. Dynamic pressure ranged from 75 psf at Mach number 0.9 to 100 psf at Mach number 1.1. The Reynolds number based on capsule diameter was about 0.88×10^6.

The force balance was operated at about 20 percent of its rated load capacity because the balance had been sized for operation at a dynamic pressure of 500 psf at a Mach number of 1.4. The readout instrumentation available did not have provision for varying the sensitivity of the balance gages. Maximum uncertainties in the data for the test Mach numbers are estimated to be as follows:

C_l	±0.04	M_∞	±0.01
C_m	±0.03	$\Omega R/V_\infty$	±0.01
C_D	±0.10	α	±0.1°
C_L	±0.10	θ_0	±0.25°
C_Y	±0.10	θ_1	±0.1°
L/D	±0.06	θ_2	±0.1°

In general, repeatability of the force data was well within the maximum uncertainties indicated.

RESULTS AND DISCUSSION

The results of the tests reported herein are presented graphically in figures 7 through 17 and are discussed in three sections: (1) rotor operating characteristics (RPM or $\Omega R/V_\infty$ vs θ_0), (2) vehicle aerodynamic characteristics, and (3) cyclic pitch control characteristics. The body-alone aerodynamic characteristics are included as a part of (2).

Rotor Operating Characteristics

No rotor-speed control problems similar to those encountered at low subsonic Mach numbers (ref. 8) were encountered in the test Mach number range, as indicated by the RPM versus θ_0 curves (fig. 7). The curves are quite smooth and become steeper as the angle of attack is increased.

For angles of attack up to 55° the rotor speed was higher at the higher Mach number. For $\alpha = 90°$, however, figure 7(a) shows that the RPM of the double-wedge configuration is lower

at $M_\infty = 1.12$ than at $M_\infty = 0.93$. This irregularity is best illustrated by the RPM versus Mach number curves shown in figure 8 for the three test configurations. A local peak in RPM occurred at about $M_\infty = 0.8$ for the short elliptic-blade configuration and at about $M_\infty = 0.9$ for the double-wedge configuration. No such peak occurred for the long elliptic-blade configuration which suggests that the peaks may be due to body interference.

The ratio of rotor tip speed to free-stream velocity is shown in figure 9 for the long and short elliptic-blade configurations. This parameter should, in the absence of body interference effects, be the same for rotors of any diameter and solidity. The data shown for $M_\infty = 1.11$ are representative of both Mach numbers tested. The correlation of the two rotor sizes is good at $\alpha = 90°$. At intermediate angles of attack (e.g., $\alpha = 55°$), however, the dimensionless tip speed of the long blade rotor is about 35 percent higher than that of the short blade rotor. At $\alpha = 15°$, the difference diminished to about 18 percent.

The dimensionless tip speeds of the short elliptic and the double-wedge blade configuration are compared in figure 10. Again the data for $M_\infty = 1.11$ are representative of both test Mach numbers. At high and intermediate angles of attack the double-wedge configuration ran substantially faster than the elliptic-blade configuration. The largest difference occurred at $\alpha = 55°$. No significant difference was noted at $\alpha = 15°$.

Vehicle Aerodynamic Characteristics

Body- The longitudinal aerodynamic characteristics of the body for the two test Mach numbers are presented in figure 11. The data show no significant changes in aerodynamic characteristics for the two test Mach numbers. The location of the moment center for all configurations tested was as shown in figure 2. With this moment center, the body was stable at angles of attack between 45° and 90° and was trimmed at about 60°. The lift-drag ratio at the stable trim point was about 0.6. The maximum lift-drag ratio was about 0.7 and occurred at $\alpha = 45°$.

Body plus rotor- The aerodynamic characteristics of the three body rotor configurations tested are presented in figures 12 through 14. The data obtained for the short elliptic-blade configuration in the high angle-of-attack range ($65° \leqslant \alpha \leqslant 90°$) are for $M_\infty = 1.01$ instead of $M_\infty = 1.11$ (fig. 13(b)). Other variations in Mach number indicated for these data resulted from difficulties in establishing the desired tunnel conditions. It is noted, however, that the changes in aerodynamic characteristics over the test Mach number range are quite small; hence the data for various Mach numbers are plotted together.

For the three body-rotor configurations tested, the rotor produced large positive pitching moments at the low and intermediate angles of attack such that all three configurations were stable at $\alpha = 35°$ and above. Longitudinal trim always occurred at an angle of attack between 75° and 80°; hence a large amount of control power would be needed to trim the vehicle at low angles of attack.

The rotor also produced large amounts of lift and drag which for a given angle of attack are roughly proportional to the rotor blade plan area. The lift and drag are not sensitive to blade pitch for angles of attack up to 45°, but near axial flight ($\alpha = 90°$) some drag modulation is available for

the blade pitch range tested. It should be noted that at $\alpha = 90°$ the drag contribution of the rotor can be reduced to nearly zero if desired by retracting the rotor.

The maximum lift-drag ratio was about 0.75 for both short blade configurations and nearly 1.0 for the long elliptic-blade configuration. These values occurred at $\alpha = 25°$ for all three configurations.

Moderate rolling moments were produced by the rotor except at about 15° to 25° and 90° angle of attack. These rolling moments were positive for clockwise rotor rotation (viewed from above) and generally increased with negative collective pitch. The effects of cyclic pitch on the rolling moment at low angles of attack are discussed under "Cyclic Pitch Control Characteristics."

Some negative side force is also produced by the rotor. The magnitude of the side-force coefficient did not exceed 0.25 except at $\alpha = 65°$ and 70° where sting interference may have significantly affected the accuracy of the data.

Effects of sting inclination- At $\alpha = 65°$ discontinuities appear in the data which are apparently caused by sting interference. When the axial mounting arrangement (fig. 5(c)) was used to test at $\alpha = 65°$, the sting inclination to the free stream was 25°. The bent balance-adapter (fig. 5(b)) allowed tests to be made at $\alpha = 65°$ with the sting parallel to the free stream. Data were obtained at this angle of attack for the double-wedge blade configuration mounted on both sting arrangements for $M_\infty = 0.93$ (fig. 12(a)) and these data show the magnitudes of the discontinuities. The data for the long elliptic-blade configuration appear to have been more strongly influenced by sting inclination than the two short-blade configurations.

Cyclic Pitch Control Characteristics

The variations in pitching-moment, rolling-moment, and side-force coefficients and the lift-drag ratio with longitudinal and lateral cyclic pitch angles are presented for $\alpha = 15°$ and 25° in figures 15 to 17, inclusive. Tests were made with the collective pitch angle held constant at -9° and in some cases at -6° as well. The cyclic pitch varied harmonically around the azimuth such that the total blade pitch at any azimuth position could be determined from $\theta(\psi) = \theta_0 - \theta_1 \sin \psi + \theta_2 \cos \psi$.

The slopes of the pitching-moment and rolling-moment curves are approximately the same for both angles of attack and both Mach numbers. These slopes are much larger (2 – 4 times larger) for the long blade configuration than for the two short blade configurations which have essentially the same control characteristics.

For all three configurations, the range of longitudinal cyclic pitch used ($-6° \leqslant \theta_1 \leqslant 7°$) was sufficient to provide roll trim at $\alpha = 15°$ and 25°. This control, however, produced very little change in the pitching moment. The same range of lateral cyclic pitch produced substantial changes in the pitching moment but not nearly enough for trim. The slopes of the pitching-moment curves indicate that pitch trim would occur for the short blades at about 20° of lateral cyclic pitch (θ_2) and at about 9° for the long blade configuration. Since only ±10° of cyclic pitch control was available, it was not possible for the short blade configurations to reach pitch trim; and because of rotor RPM limitations, it was not possible for the long blade configuration to achieve pitch trim.

Increasing θ_2 beyond 6° caused the rotor speed to become dangerously low; hence no data were taken beyond that point. For the range of cyclic pitch tested, varying lateral cyclic pitch had relatively little effect on the rolling moment. The lift-drag ratio was not significantly affected by variations in either lateral or longitudinal cyclic pitch.

CONCLUSIONS

Wind-tunnel tests have been made of several configurations of a rotor entry vehicle model to establish the aerodynamic performance characteristics of an unpowered rotor at Mach numbers from $M_\infty = 0.91$ to 1.11. The tests were made with two different blade sections, a 20-percent modified ellipse and a 20-percent double wedge, and two different blade lengths for the elliptic section. The two blade lengths gave rotor-to-body diameter ratios of 3 and 4. The double-wedge blades were of the shorter length. Blade collective pitch was used to control rotor speed at all model attitudes. Cyclic pitch control characteristics were studied for several blade collective pitch angles.

The results of these tests indicate the following:

1. No rotor speed control problems were encountered in the test Mach number range.

2. For the angle of attack range $65° \leqslant \alpha \leqslant 90°$ a local peak occurred in the RPM versus Mach number curves for the two short blade configurations. The peak occurred at $M_\infty = 0.8$ for the short elliptic-blade configuration and at $M_\infty = 0.9$ for the double-wedge blade configuration. No peak occurred in the RPM curve for the long elliptic-blade configuration.

3. Two short blade rotor configurations that differed only in blade section shape had essentially the same aerodynamic characteristics. The long blade configuration had much larger forces and moments.

4. Effects of Mach number on the aerodynamic forces and moments were small.

5. For all three configurations tested the rotor produced large positive pitching moments at low and intermediate angles of attack which could not be trimmed with the cyclic pitch control. All configurations were stable at $\alpha = 35°$ and above. Longitudinal trim occurred at an angle of attack between 75° and 80°.

6. The maximum lift-drag ratio was about 0.75 for the short blade configurations and nearly 1.0 for the long blade configuration. These values occurred at $\alpha = 25°$ for all three configurations.

7. Moderate rolling moments were produced by the rotor and generally increased with negative collective pitch. These moments could be trimmed out with the longitudinal cyclic pitch control.

Ames Research Center
National Aeronautics and Space Administration
Moffett Field, Calif., 94035, Sept. 15, 1970

REFERENCES

1. Haig, C. R., Jr.: The Use of Rotors for the Landing and Reentry Braking of Manned Spacecraft. IAS Paper No. 60-17, Jan. 1960.

2. Fletcher, C. J.; and Tesch, E. C., Jr.: ROR-Chute Concept for Recovery Systems. Thiokol Chemical Corp. TR 3740, Jan. 1961.

3. Kretz, M.: Application of Rotary Wing Techniques to Atmospheric Re-Entry and Launch Vehicle Recovery Problems. Paper presented at the European Symposium on Space Technology, London, England, June 1961.

4. Barzda, J. J.; and Schultz, E. R.: Test Results of Rotary-Wing Decelerator Feasibility Studies for Capsule Recovery Applications. SAE Paper No. 756D, Sept. 1963.

5. Ham, Norman D.: An Experimental and Theoretical Investigation of a Supersonic Rotating Decelerator. J. Am. Helicopter Soc., vol. 8, no. 1 Jan. 1963, pp. 8-18.

6. Levin, Alan D.; and Smith, Ronald C.: An Analytical Investigation of the Aerodynamic and Performance Characteristics of an Unpowered Rotor Entry Vehicle. NASA TN D-4537, 1968.

7. Smith, Ronald C.; and Levin, Alan D.: Heat Transfer Measurements on the Rotor Blade of a Rotor Entry Vehicle Model. NASA TN D-4065, 1967.

8. Smith, Ronald C.; and Levin, Alan D.: Experimental Aerodynamic Performance Characteristics of a Rotor Entry Vehicle Configuration – I – Subsonic. NASA TN D-7046

9. Hollrock, Richard: Rotor Re-Entry Vehicle Wind Tunnel Model. Final Report. Kaman Aircraft Corp. Rep. R-581, May 1965.

TABLE 1.- SCOPE OF THE BODY-ROTOR INVESTIGATION

Config. \ Mach No.	PART I		PART II		PART III	
	0.3	0.7	0.9	1.1	1.6	3.5
B	○	○	○	○	○	○
BR_d	○	○	○	○	○	○
$BR_e{}^L$	○	○	○	○		
BR_e	○	○	○	○	○	○

Configuration Code:

B - Body

R_d - Short double-wedge blade section (R/d = 1.5)

$R_e{}^L$ - Long elliptic-blade section (R/d = 2.0)

R_e - Short elliptic-blade section (R/d = 1.5)

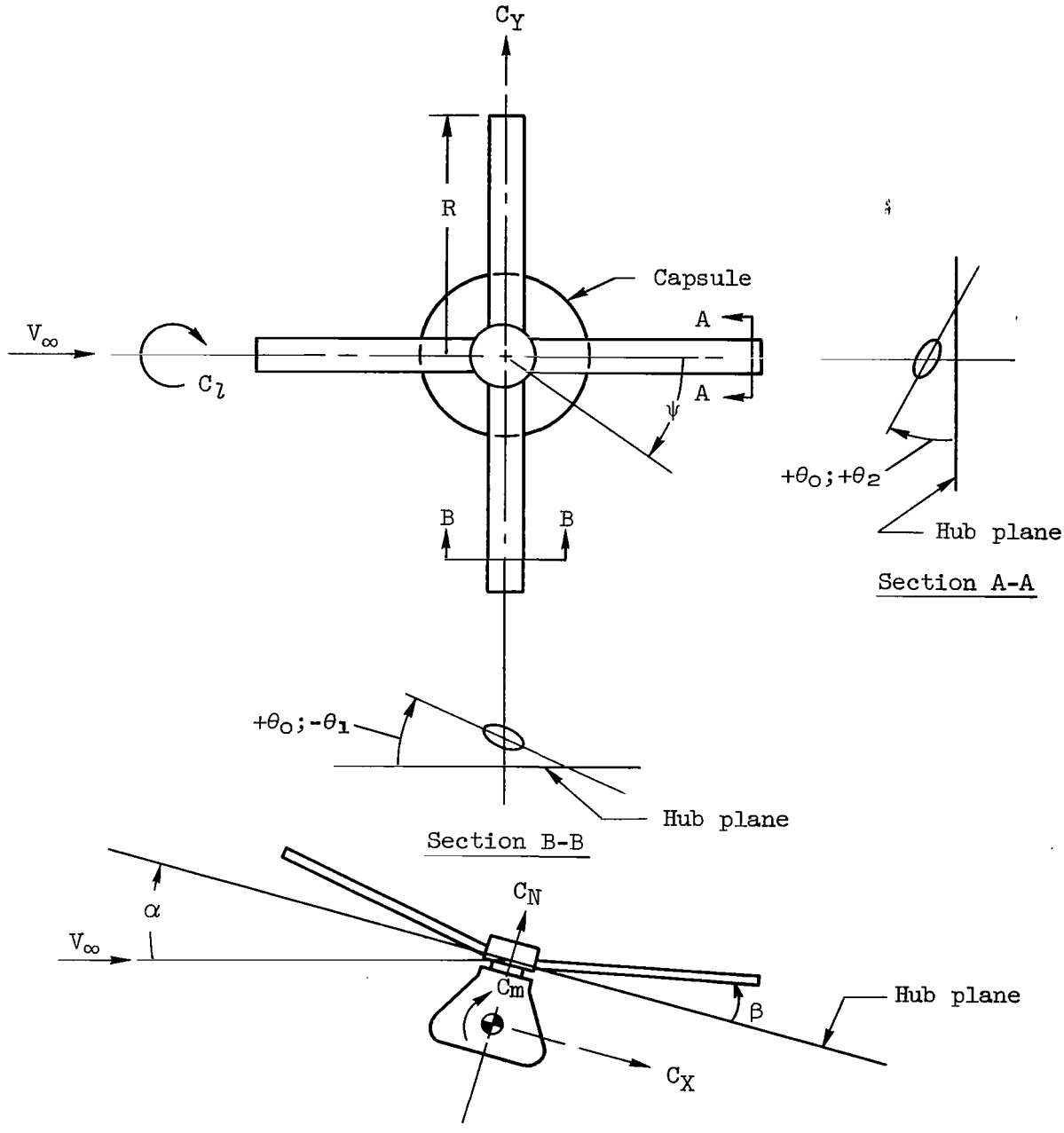

Figure 1.- Notation showing direction of forces and angles.

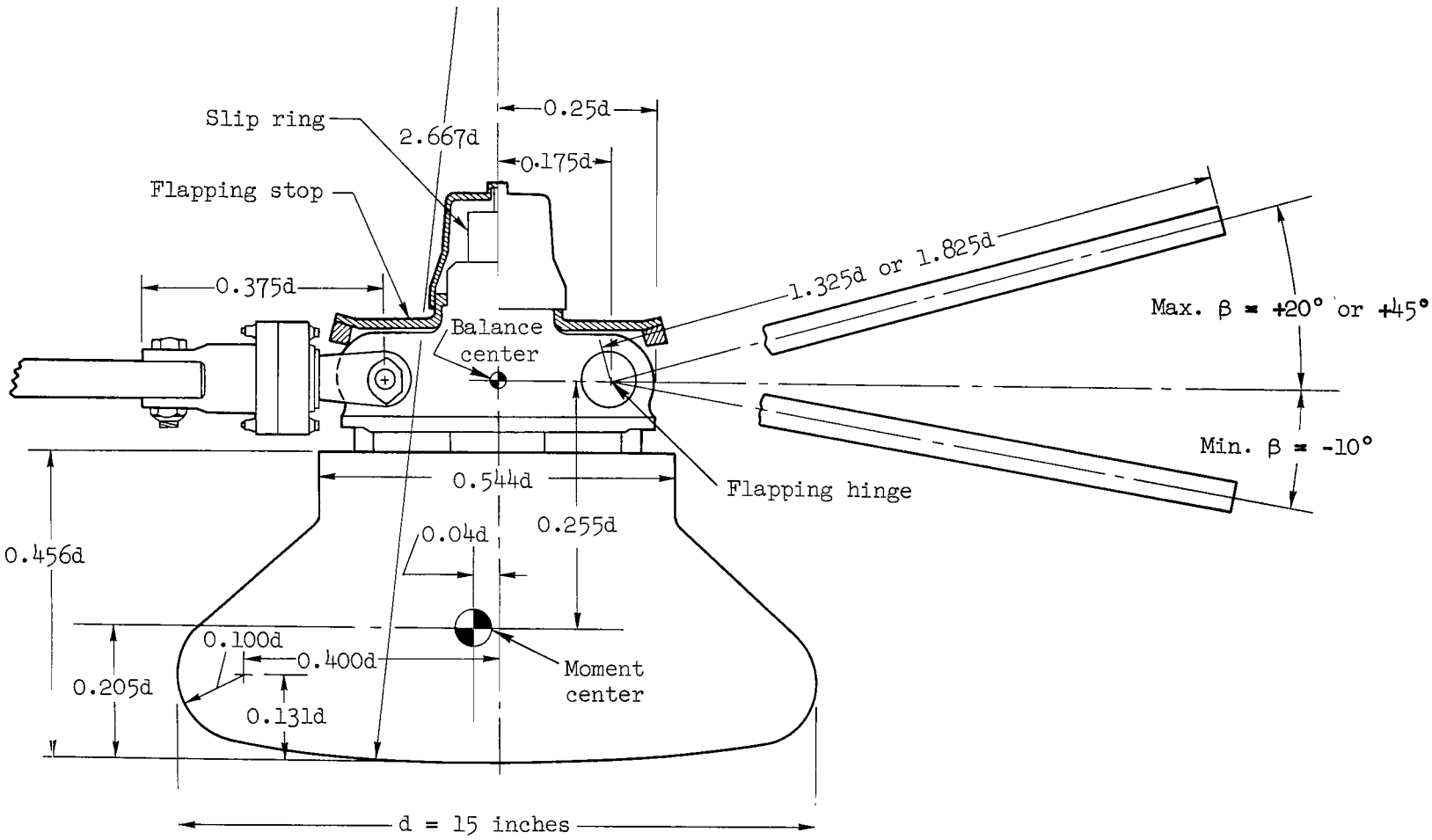

Figure 2.- Geometry of the rotor entry vehicle wind tunnel model.

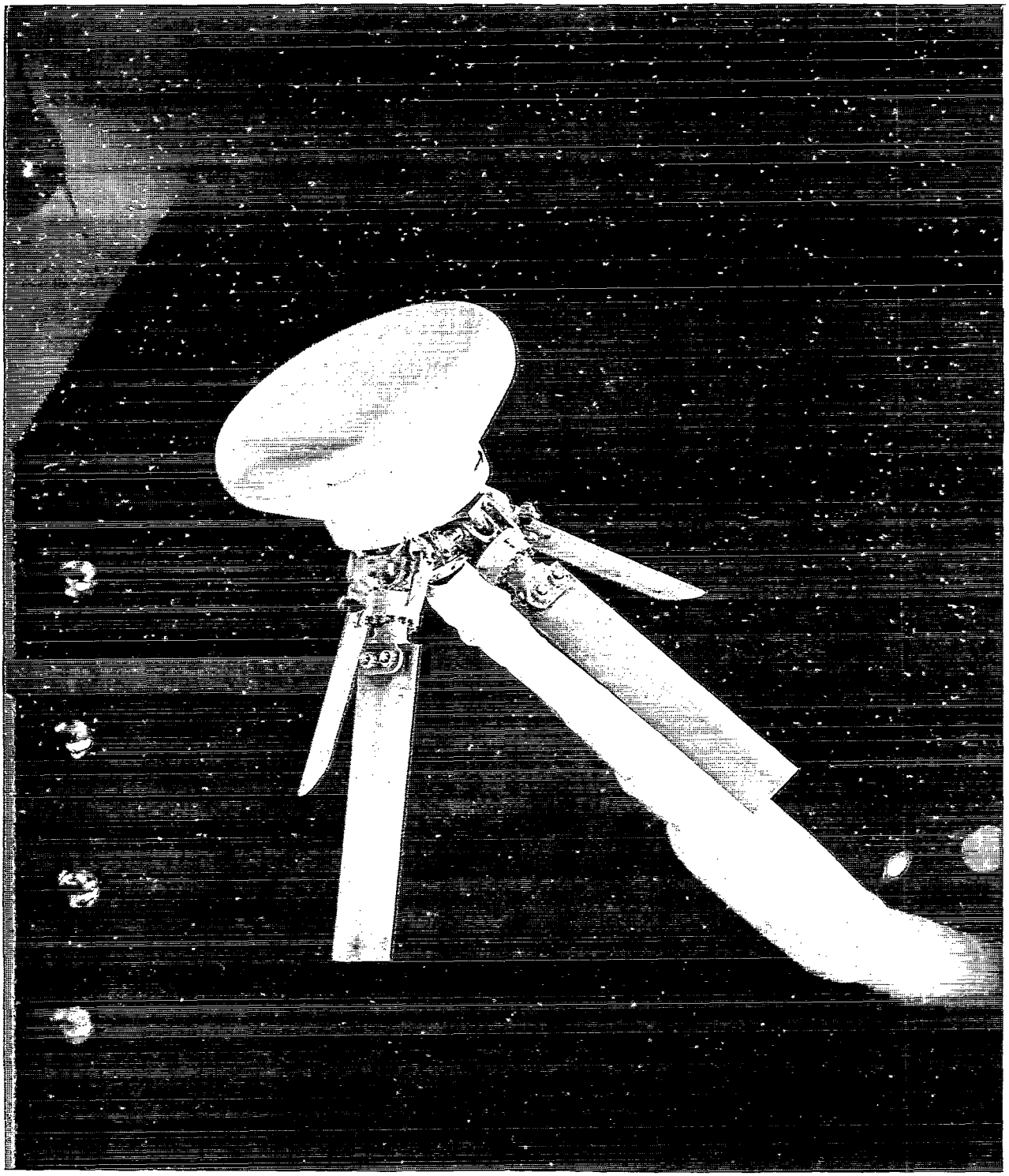

Figure 3.- Rotor entry vehicle model mounted in the Langley Transonic Dynamics Tunnel; arrangement shown for the range $35^{\circ} < \alpha < 65^{\circ}$.

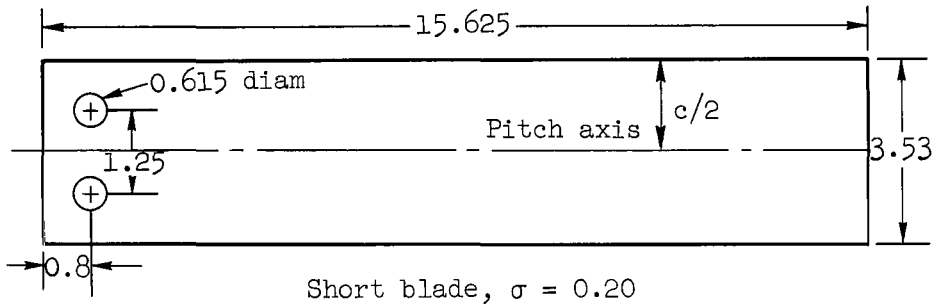

Short blade, $\sigma = 0.20$

Note: All dimensions are in inches

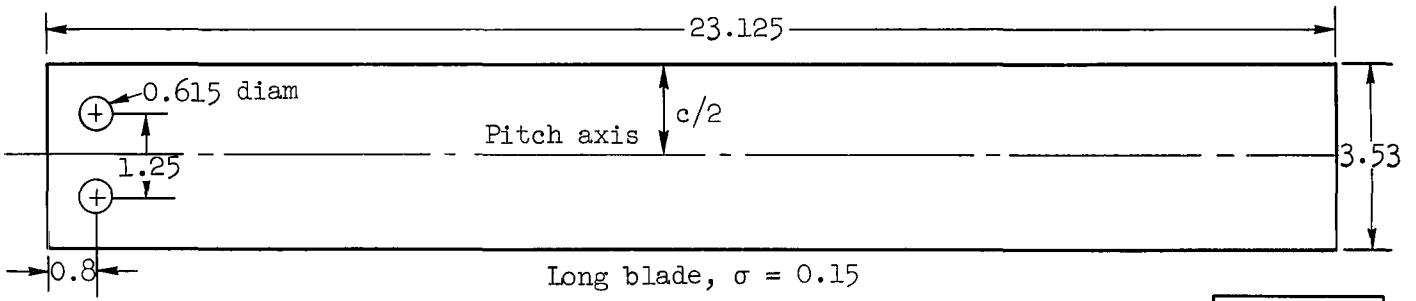

Long blade, $\sigma = 0.15$

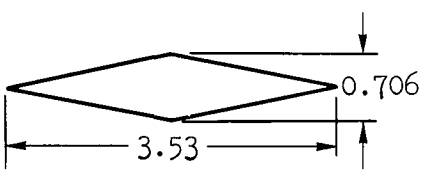

Wedge Section

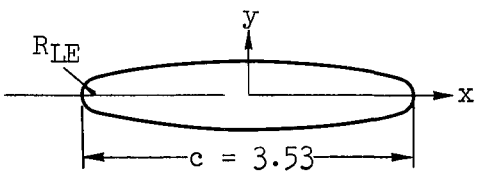

Modified ellipse section

MOD. ELLIPSE COORDINATES	
± x/c	± y/c
0	0.1000
0.0417	0.0994
0.0834	0.0985
0.1250	0.0969
0.1667	0.0950
0.2083	0.0925
0.2500	0.0890
0.2917	0.0840
0.3333	0.0777
0.3750	0.0702
0.4167	0.0606
0.4583	0.0481
0.4688	0.0440
0.4792	0.0388
0.4896	0.0299

$$\frac{R_{LE}}{c} = 0.0469$$

Figure 4.- Rotor entry vehicle blade geometry.

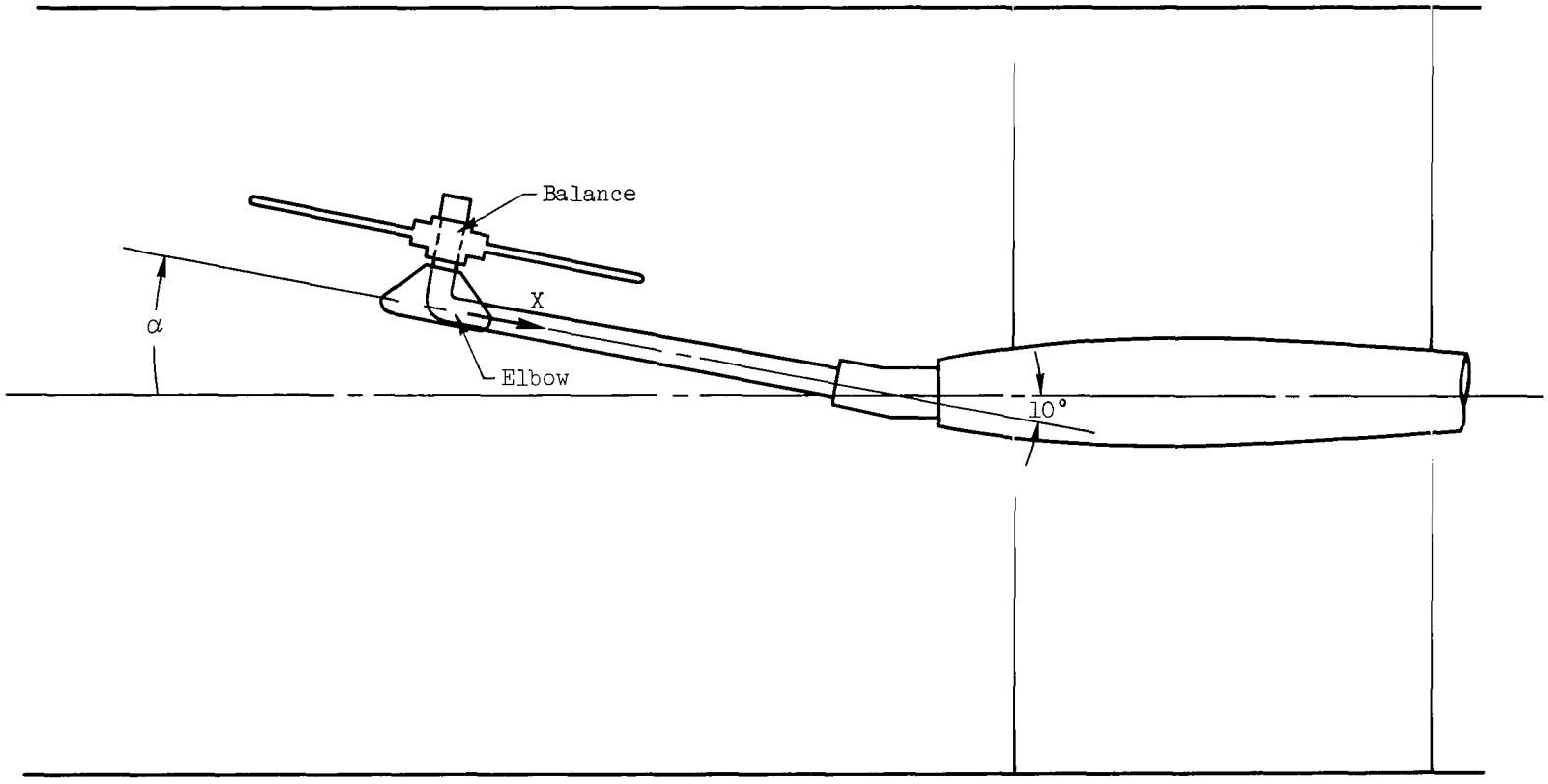

(a) $\alpha = 0^{\circ}$ to 25°

Figure 5.- Model mounting arrangements.

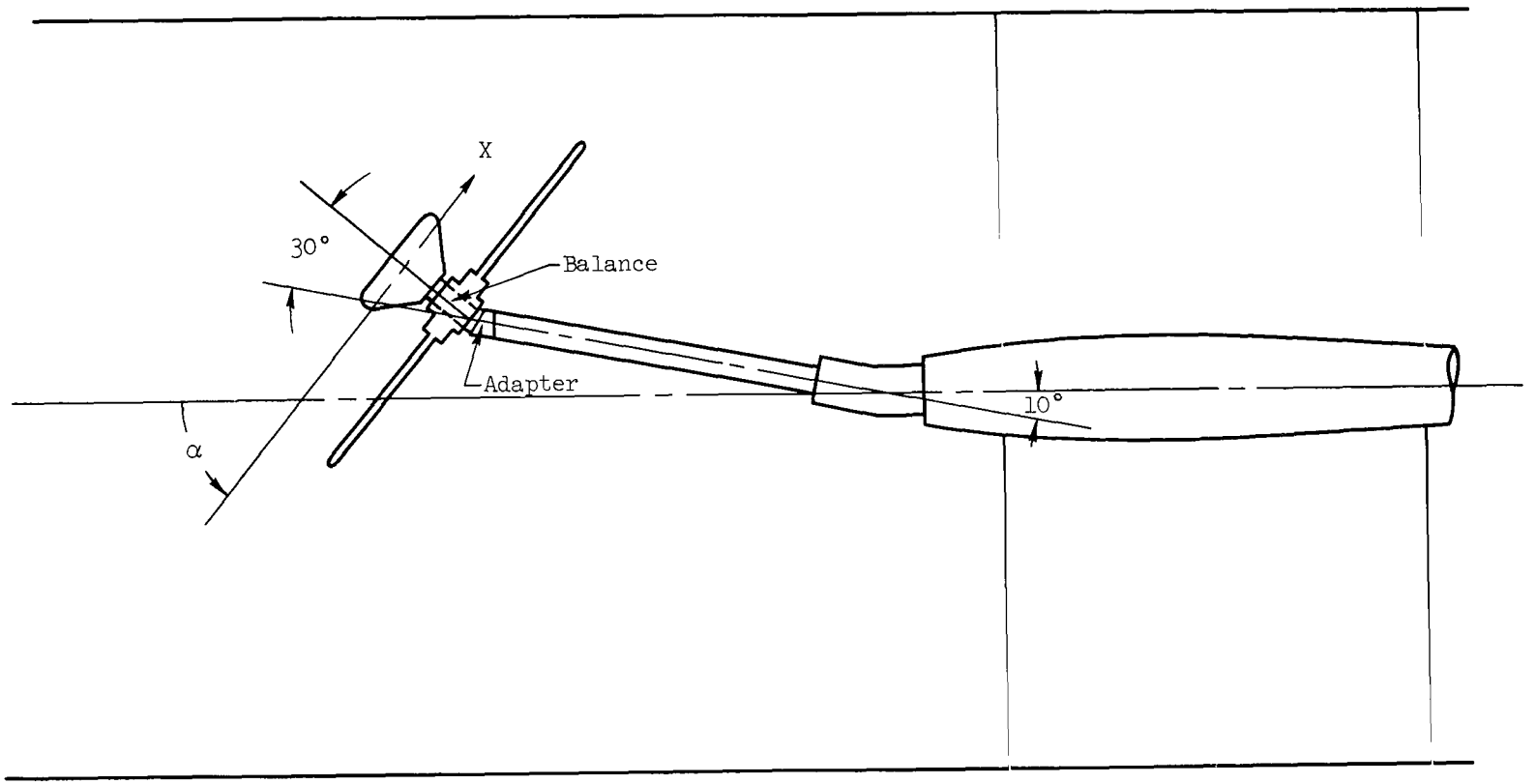

(b) $\alpha = 35^{\circ}$ to 65°

Figure 5.- Continued.

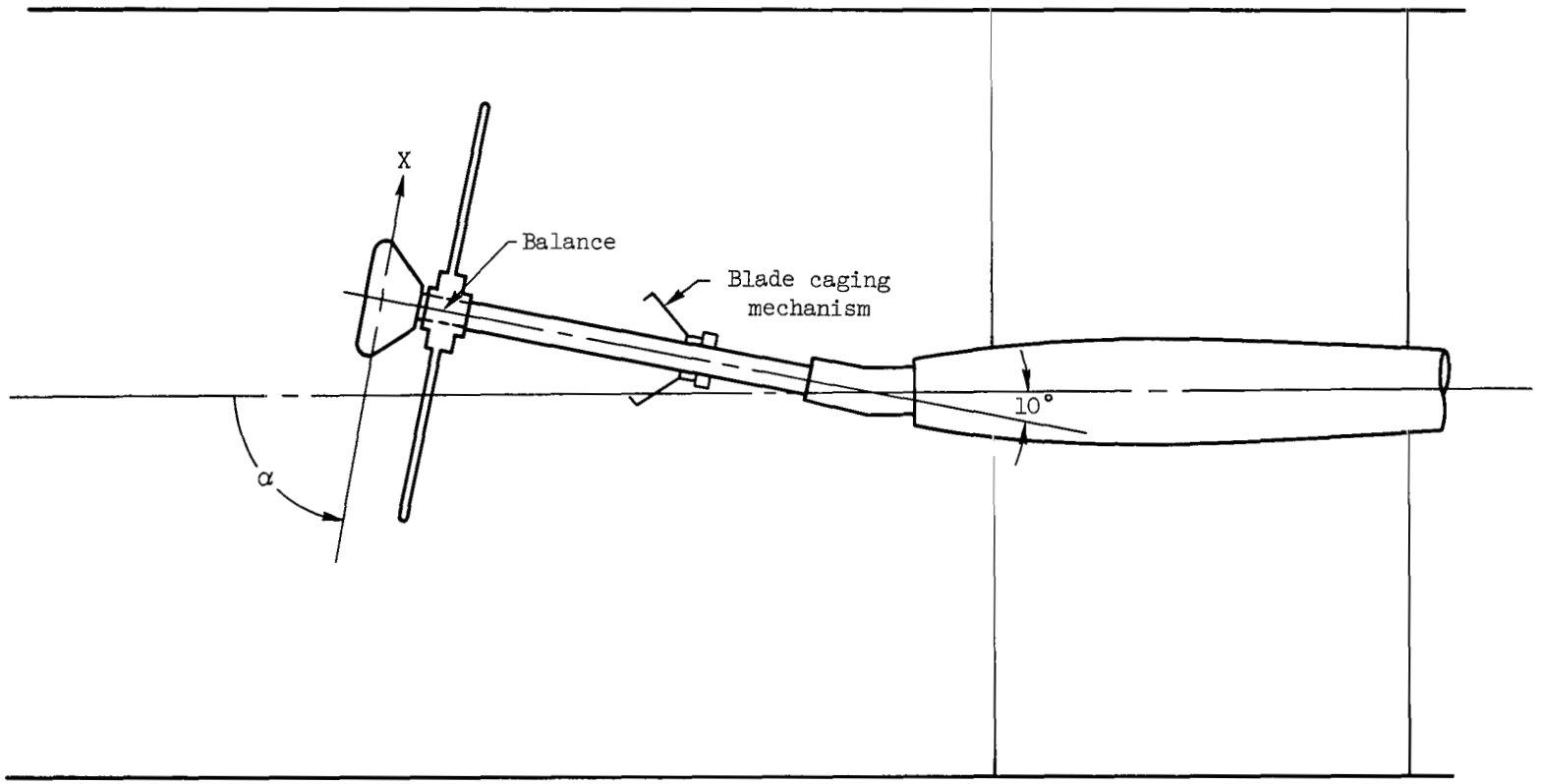

(c) $\alpha = 65^{\circ}$ to 90°

Figure 5.- Concluded.

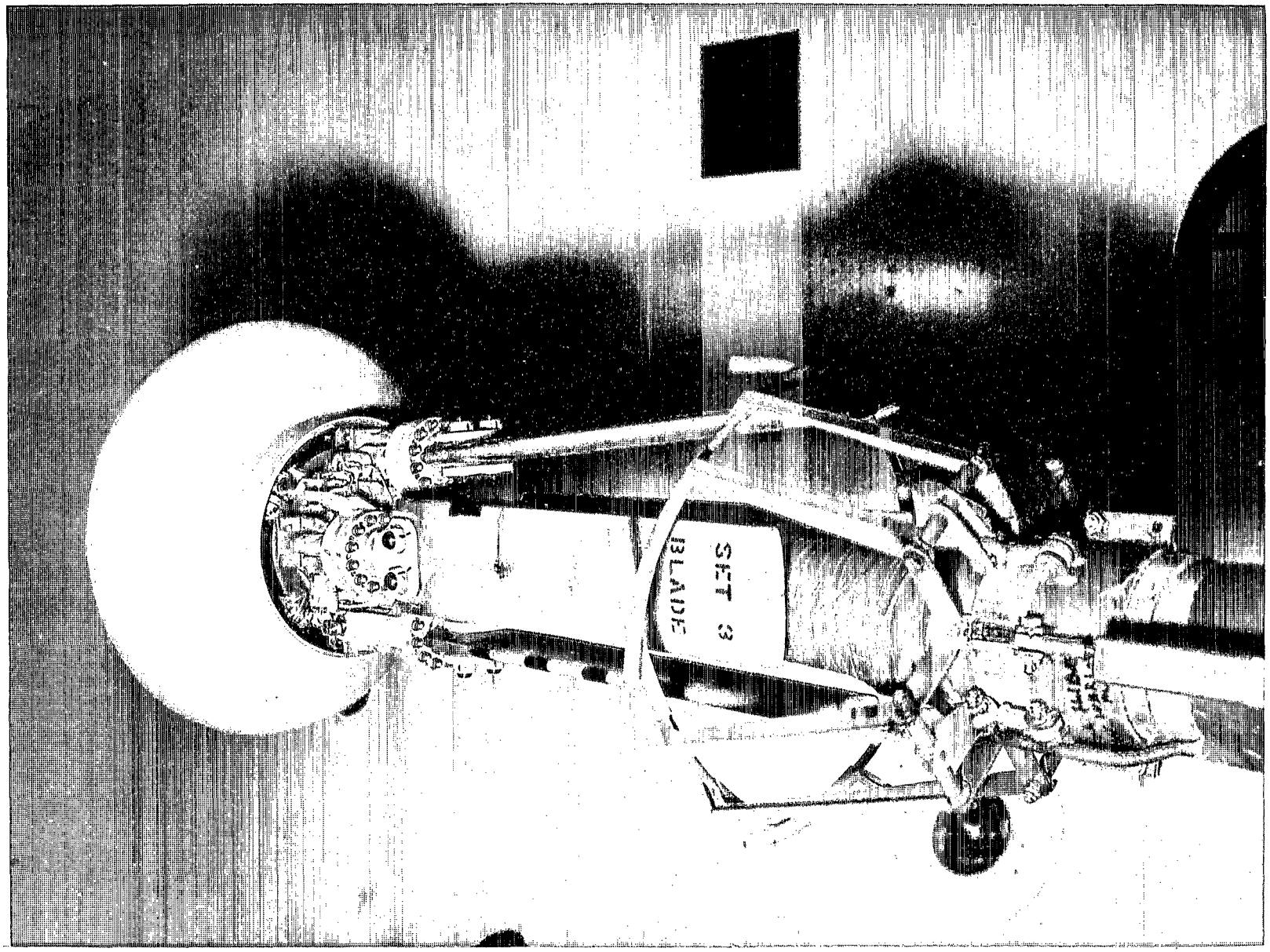

Figure 6.- Model with rotor blades in the caged position.

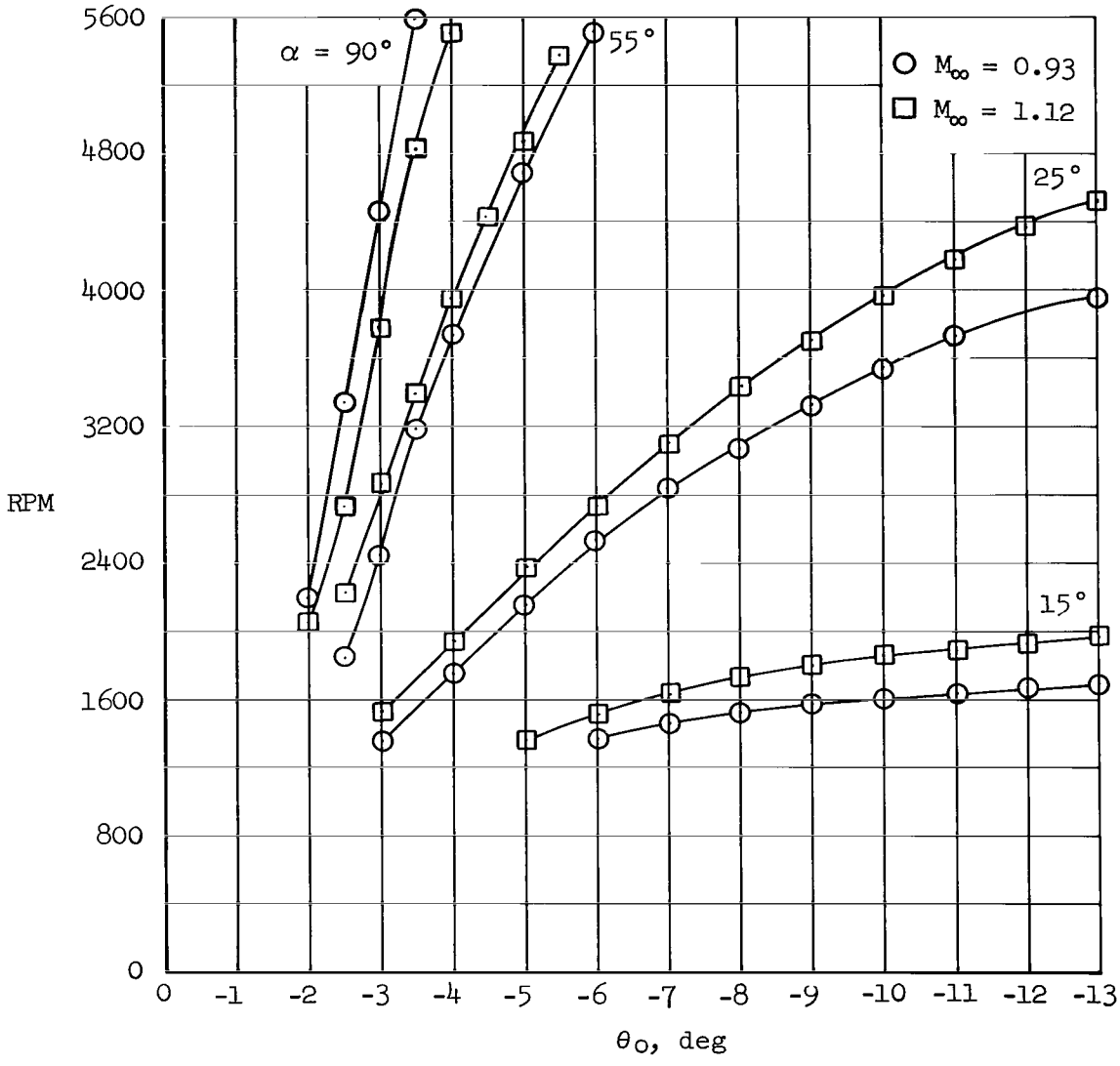

(a) Double-wedge blade

Figure 7.- Effect of free-stream Mach number on rotor operating characteristics; $\theta_1 = 0^\circ$, $\theta_2 = 0^\circ$.

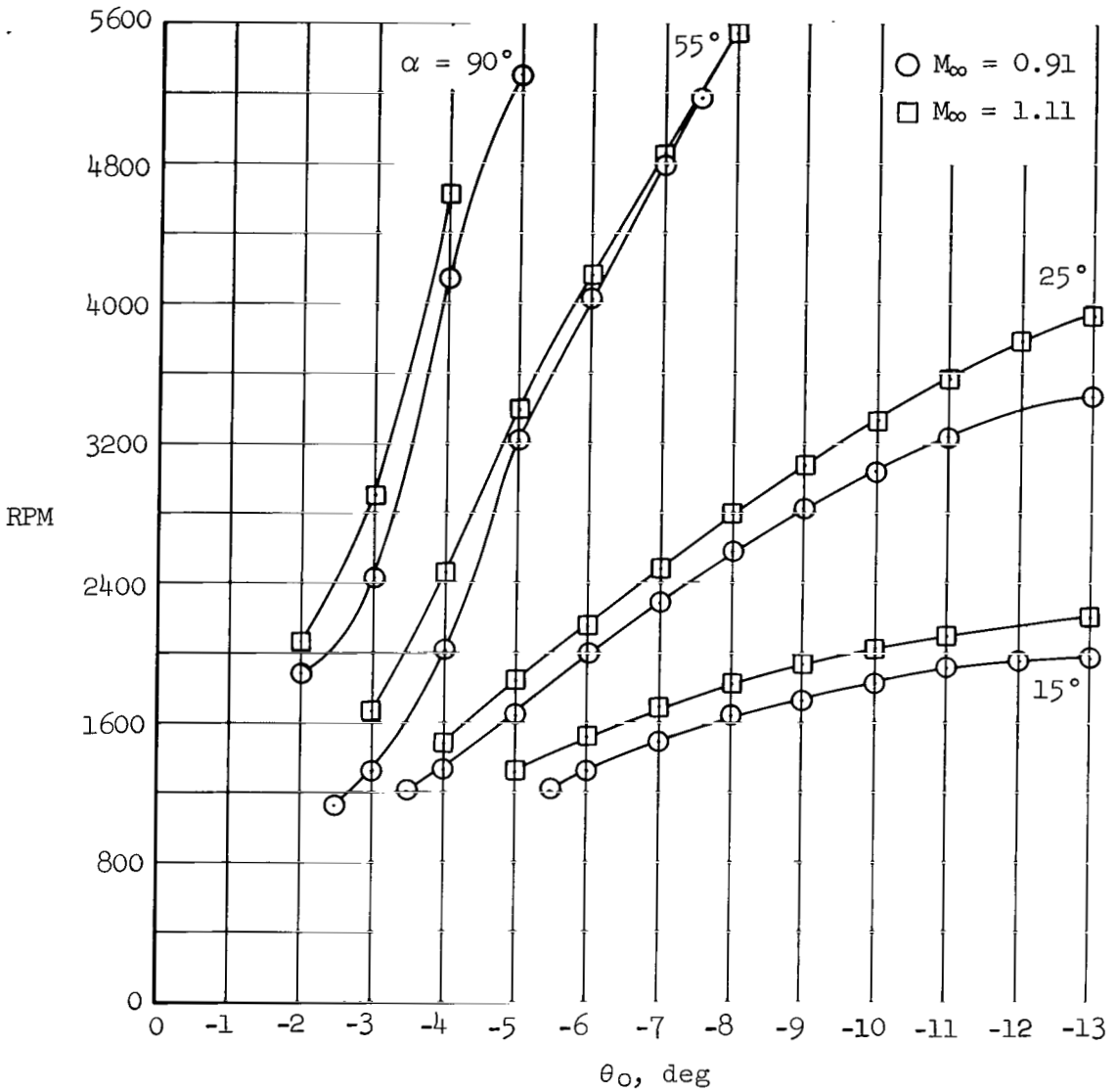

(b) Short elliptic blade

Figure 7.- Continued.

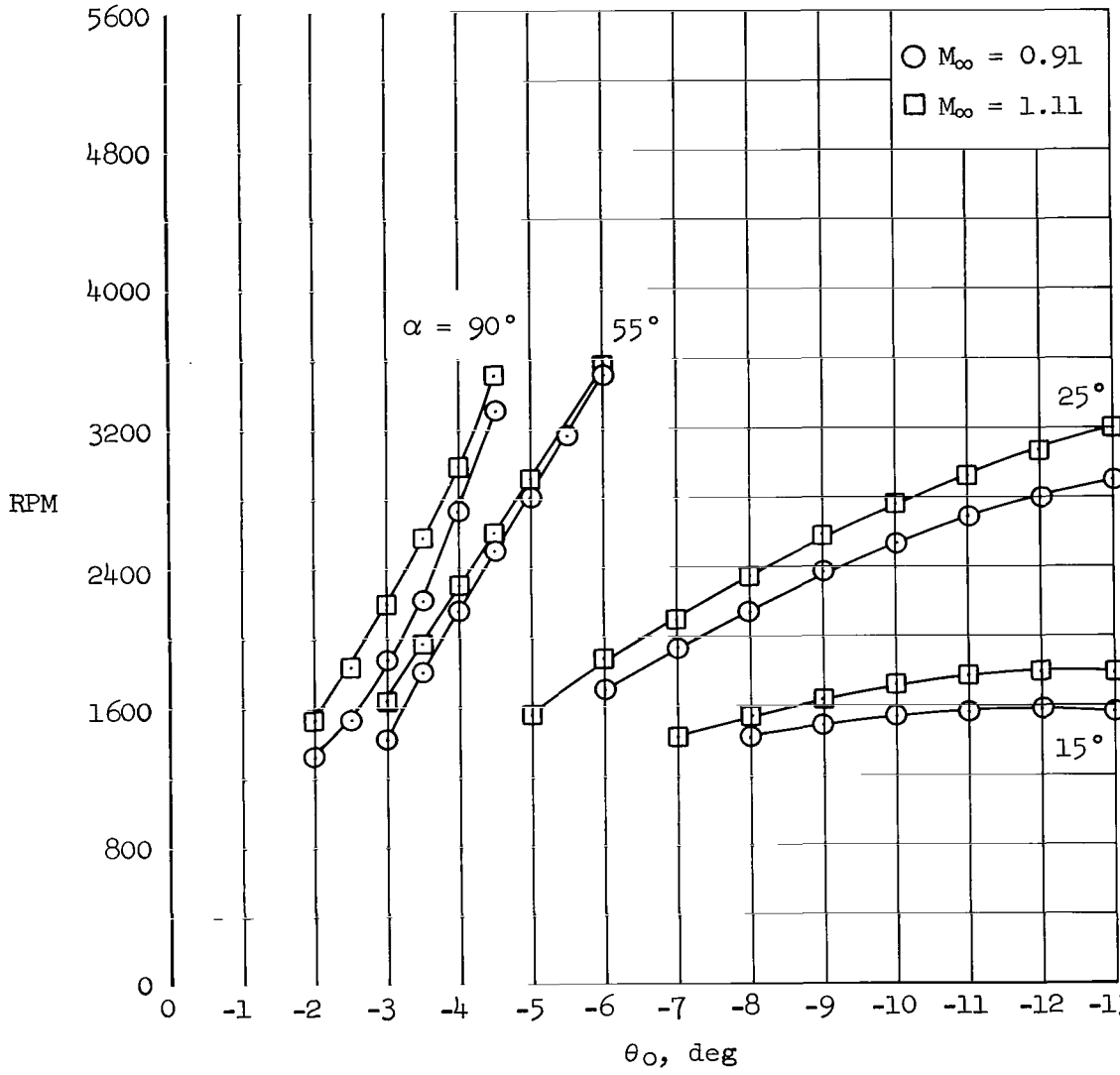

(c) Long elliptic blade

Figure 7.- Concluded.

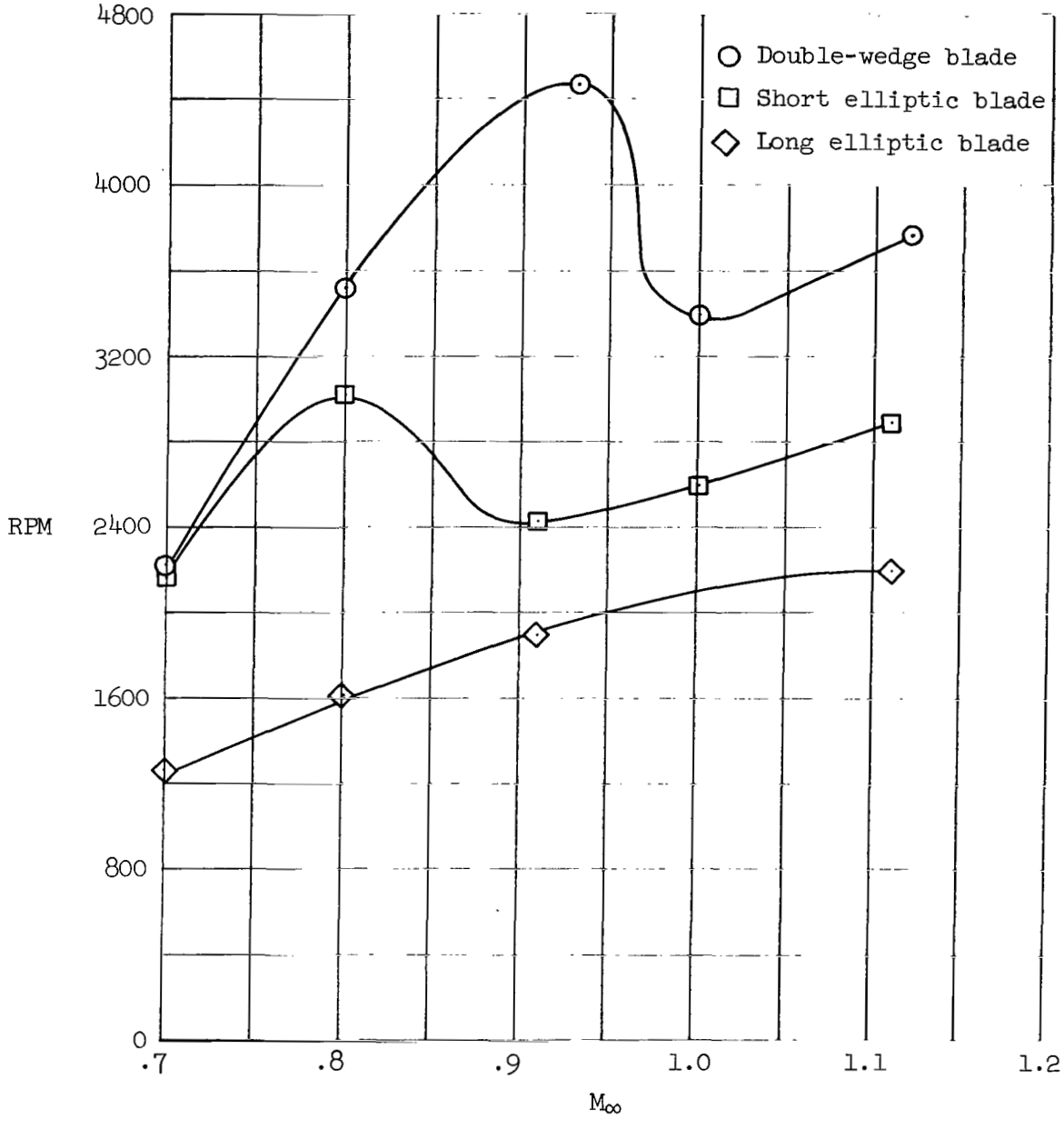

Figure 8.- RPM versus free-stream Mach number; $\alpha = 90^\circ$, $\theta_0 = -3^\circ$, $\theta_1 = 0^\circ$, $\theta_2 = 0^\circ$.

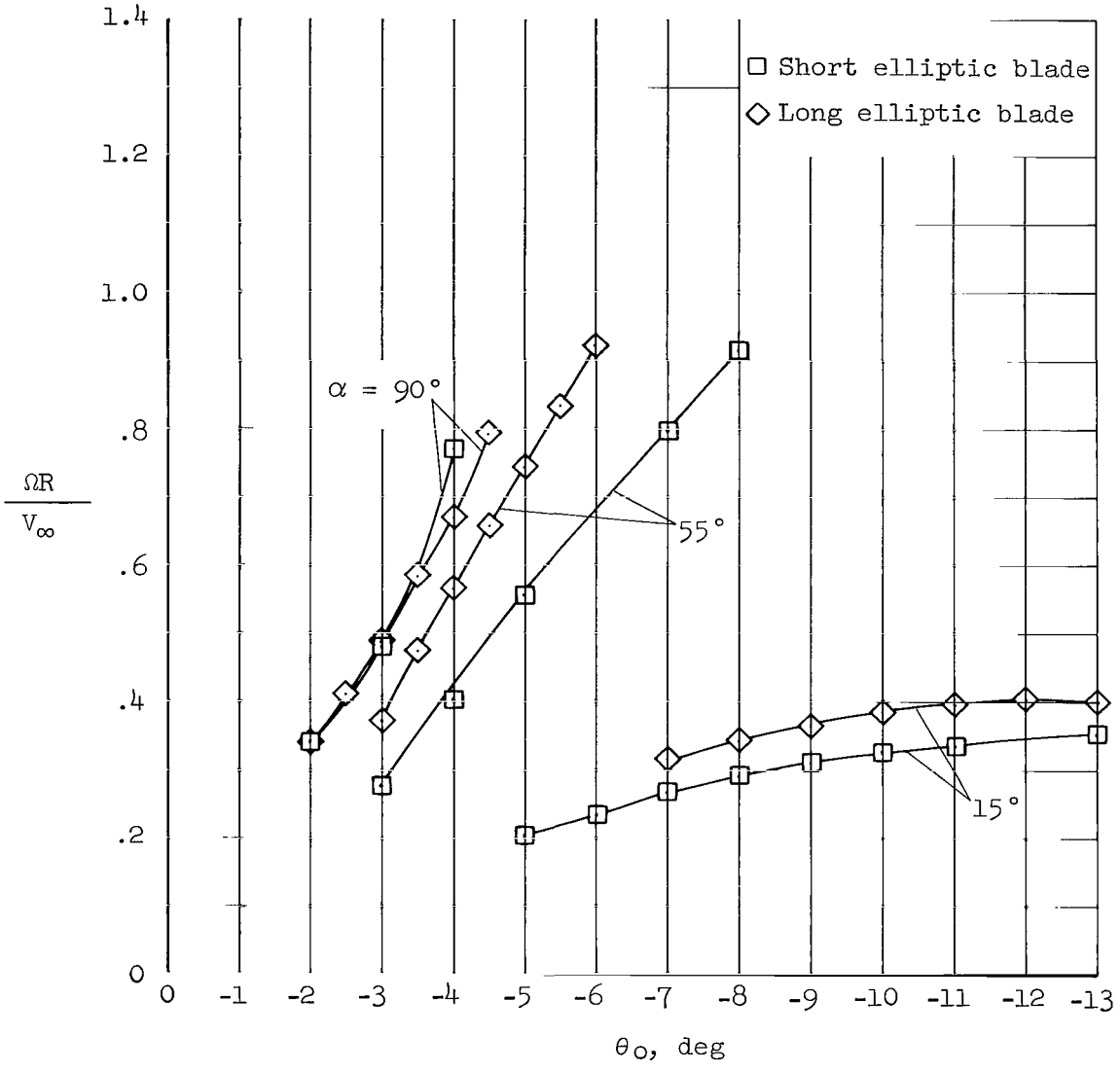

Figure 9.- Effect of blade length on rotor operating characteristics; $M_\infty = 1.11$, $\theta_1 = 0^\circ$, $\theta_2 = 0^\circ$.

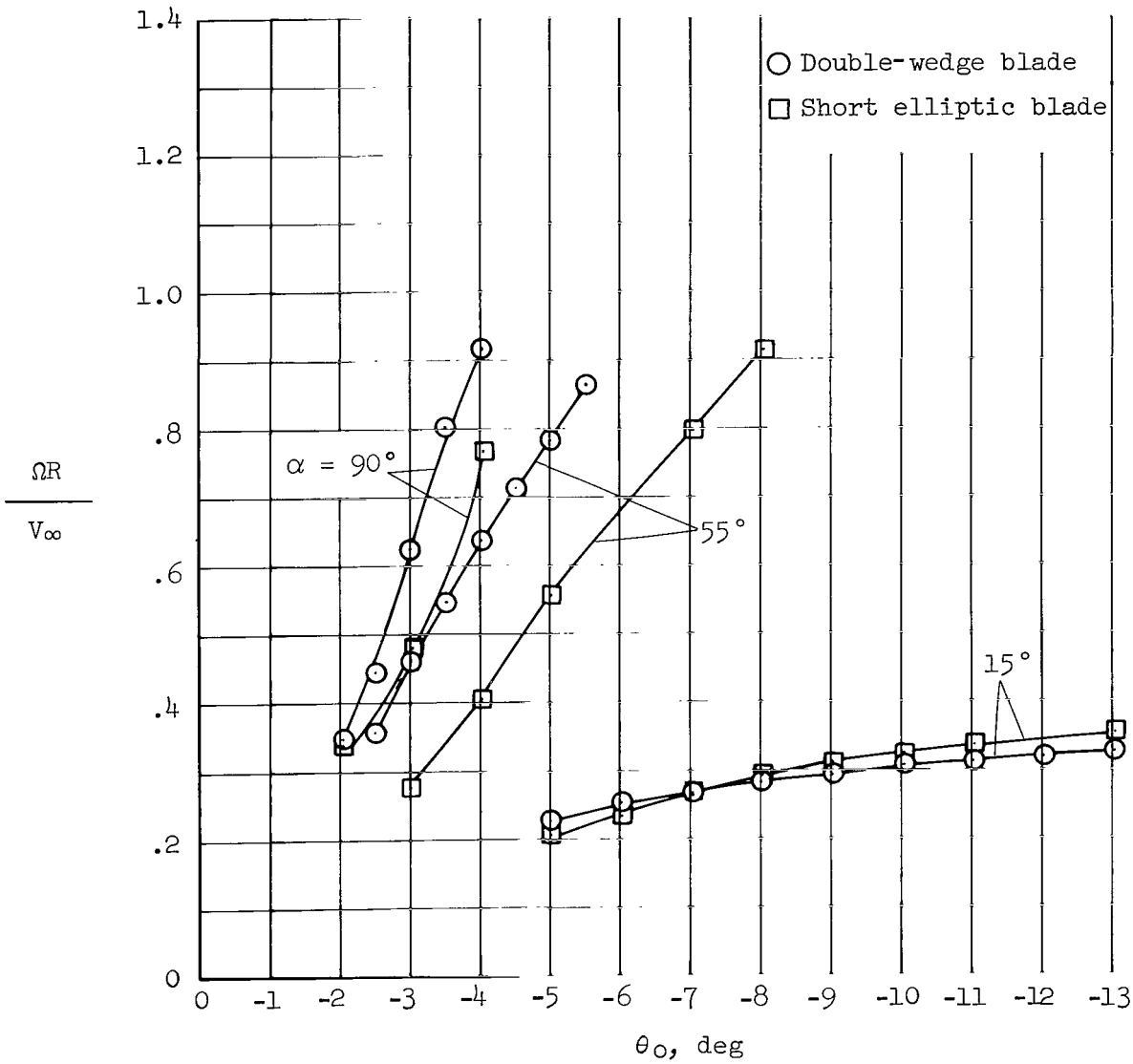

Figure 10.- Effect of blade section on rotor operating characteristics; $M_\infty = 1.11$, $\theta_1 = 0^\circ$, $\theta_2 = 0^\circ$.

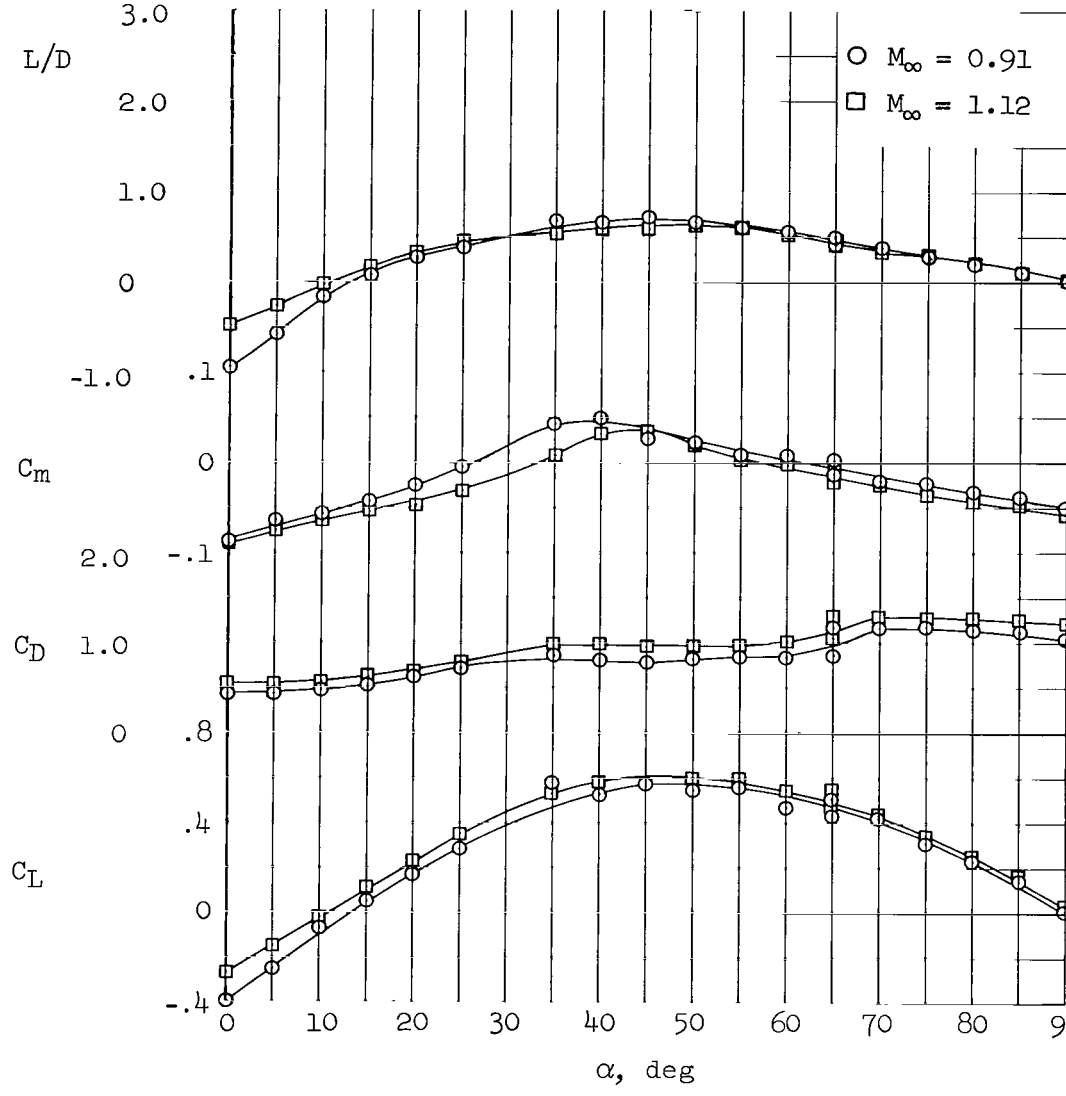

Figure 11.- Body-alone longitudinal aerodynamic characteristics.

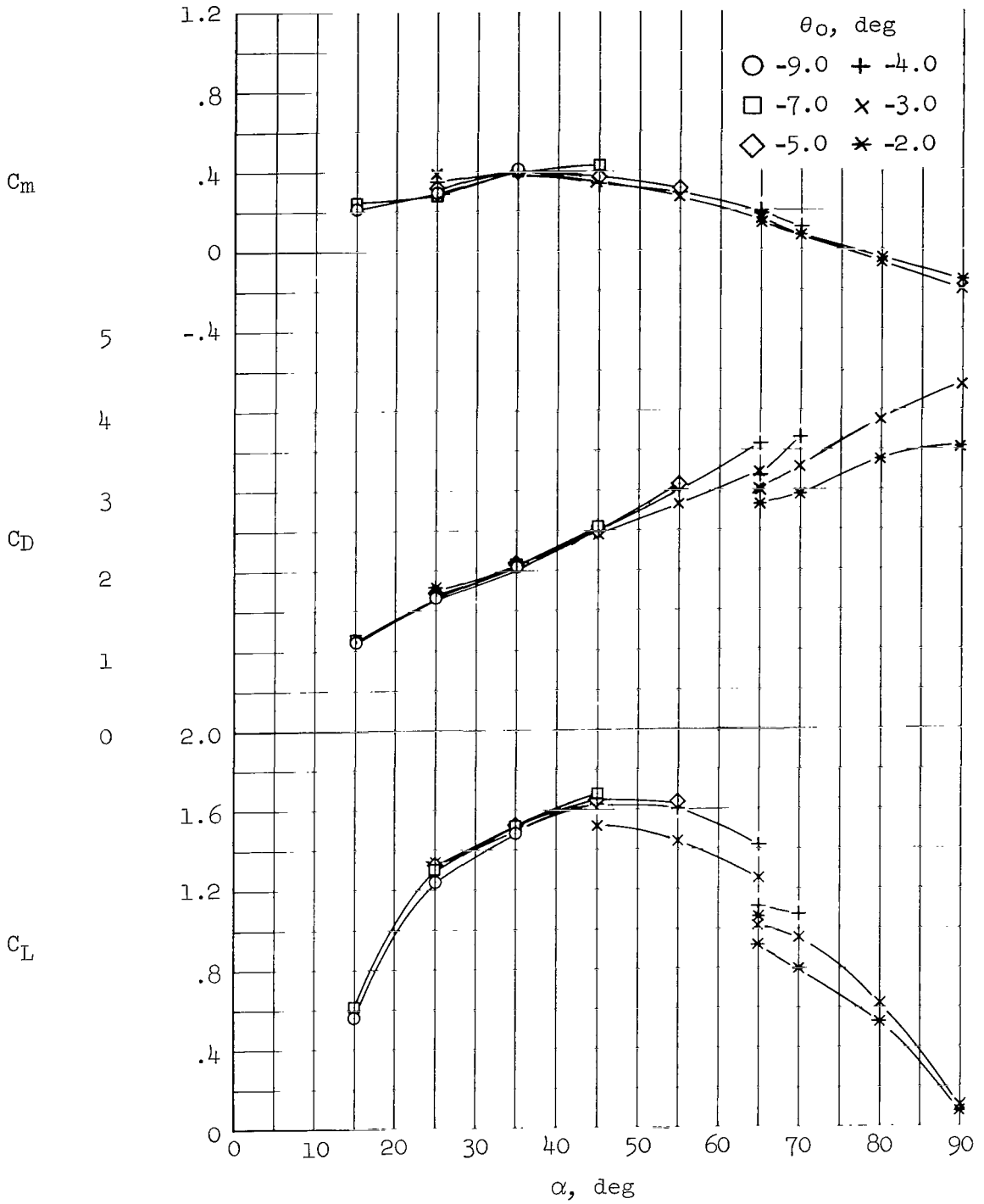

(a) $M_\infty = 0.93$

Figure 12.- Aerodynamic characteristics of the body-rotor configuration, double-wedge blades; $\theta_1 = 0^o$, $\theta_2 = 0^o$.

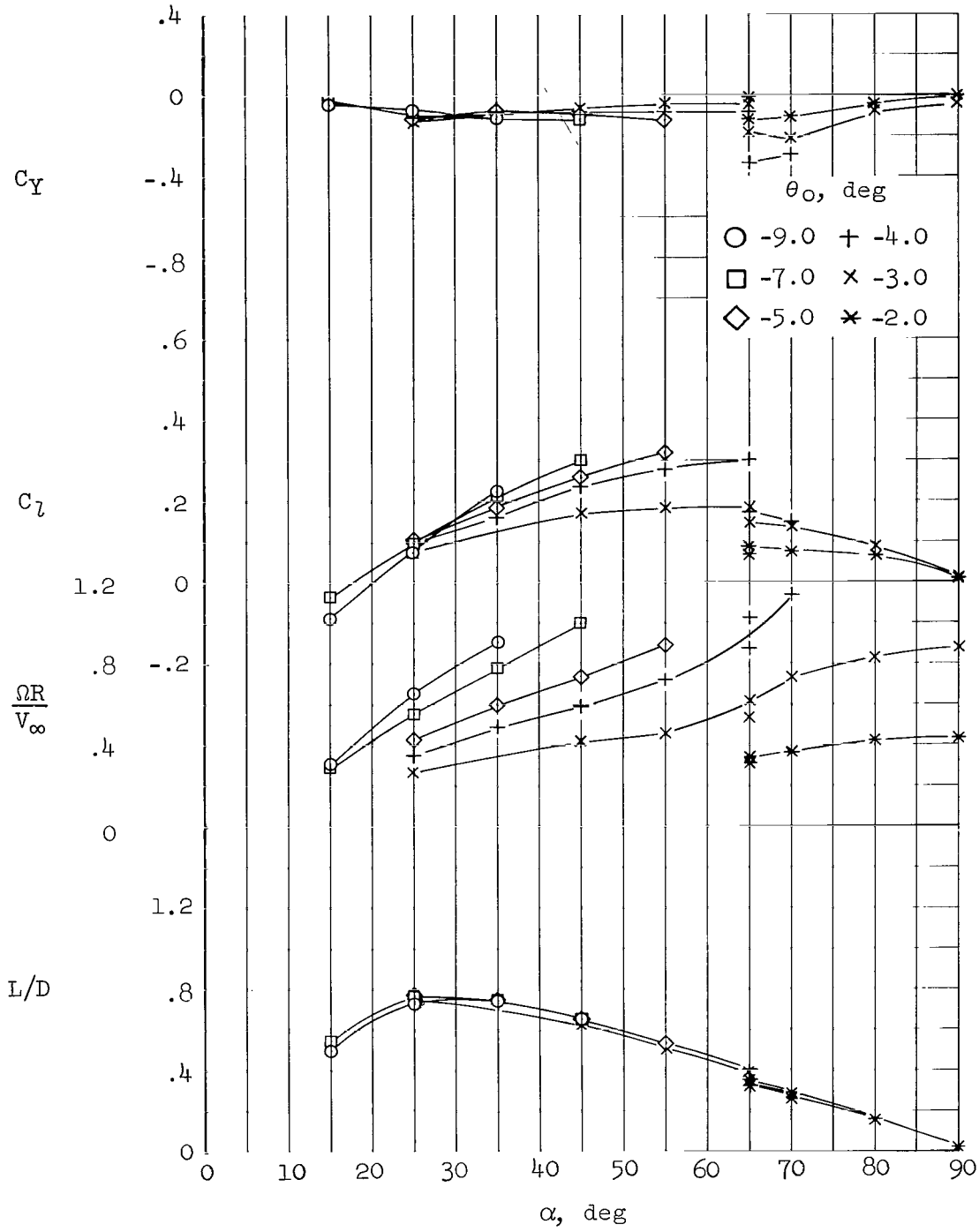

(a) M_∞ = 0.93 - Concluded.

Figure 12.- Continued.

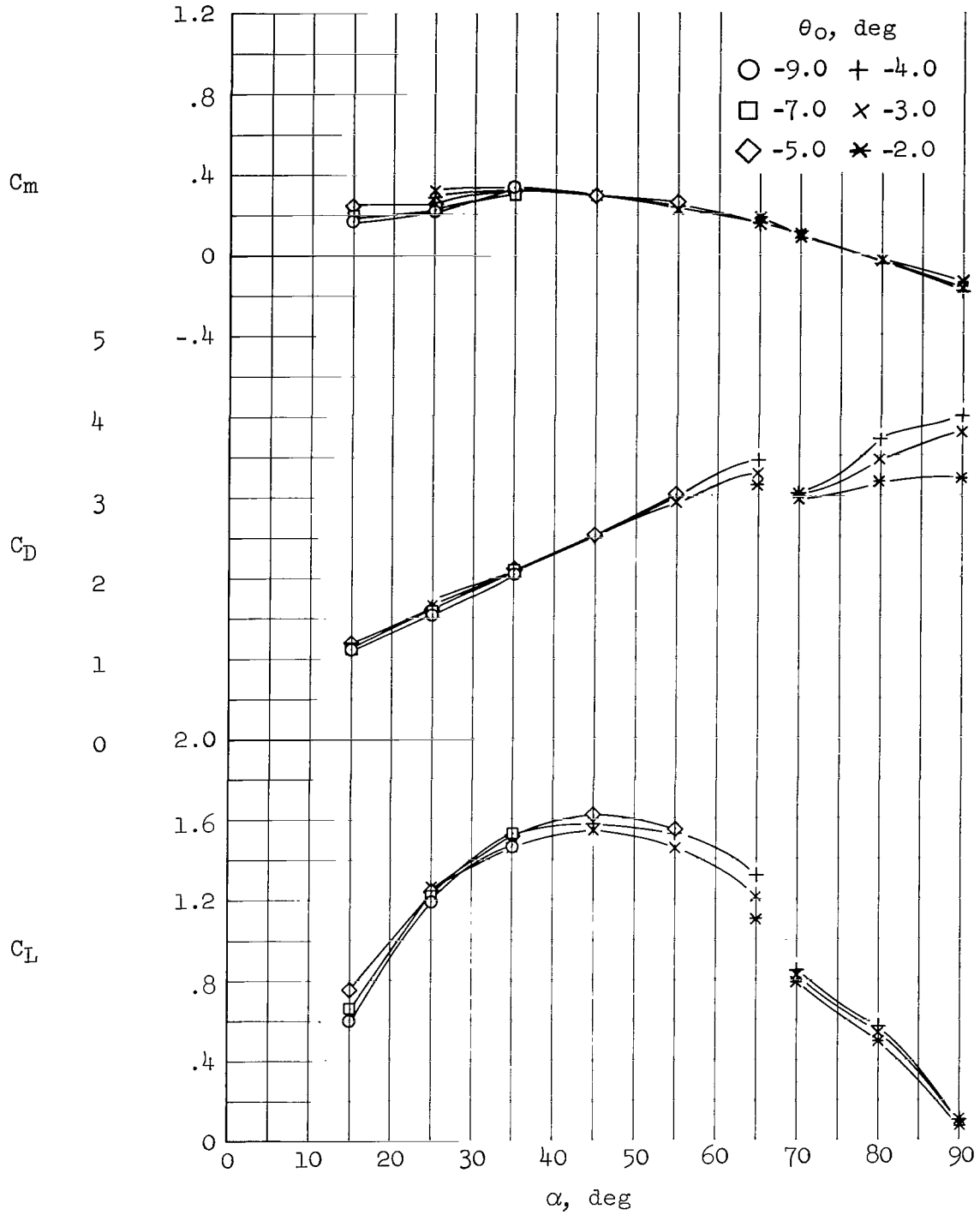

(b) $M_\infty = 1.12$

Figure 12.- Continued.

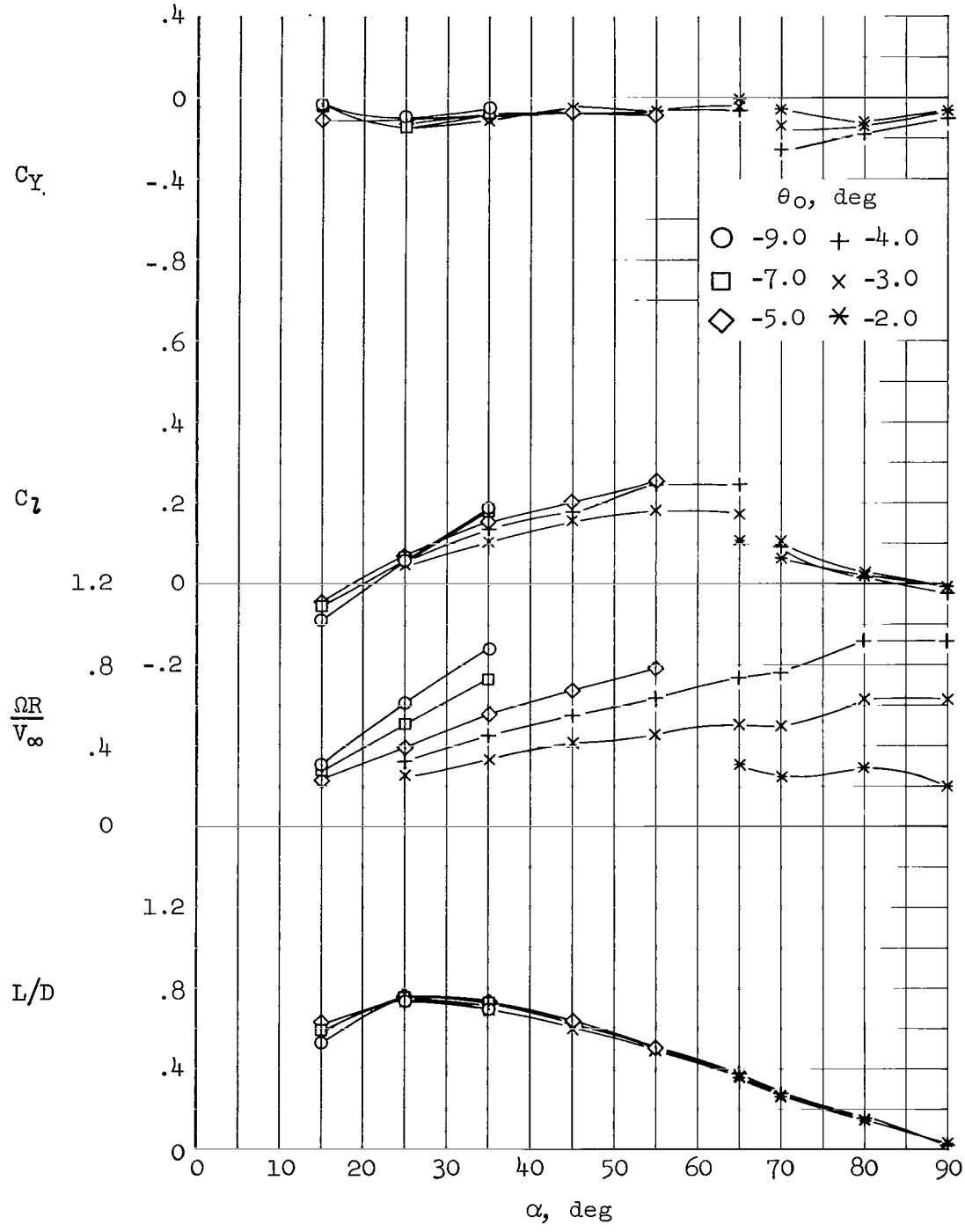

(b) M_∞ = 1.12 - Concluded.

Figure 12.- Concluded.

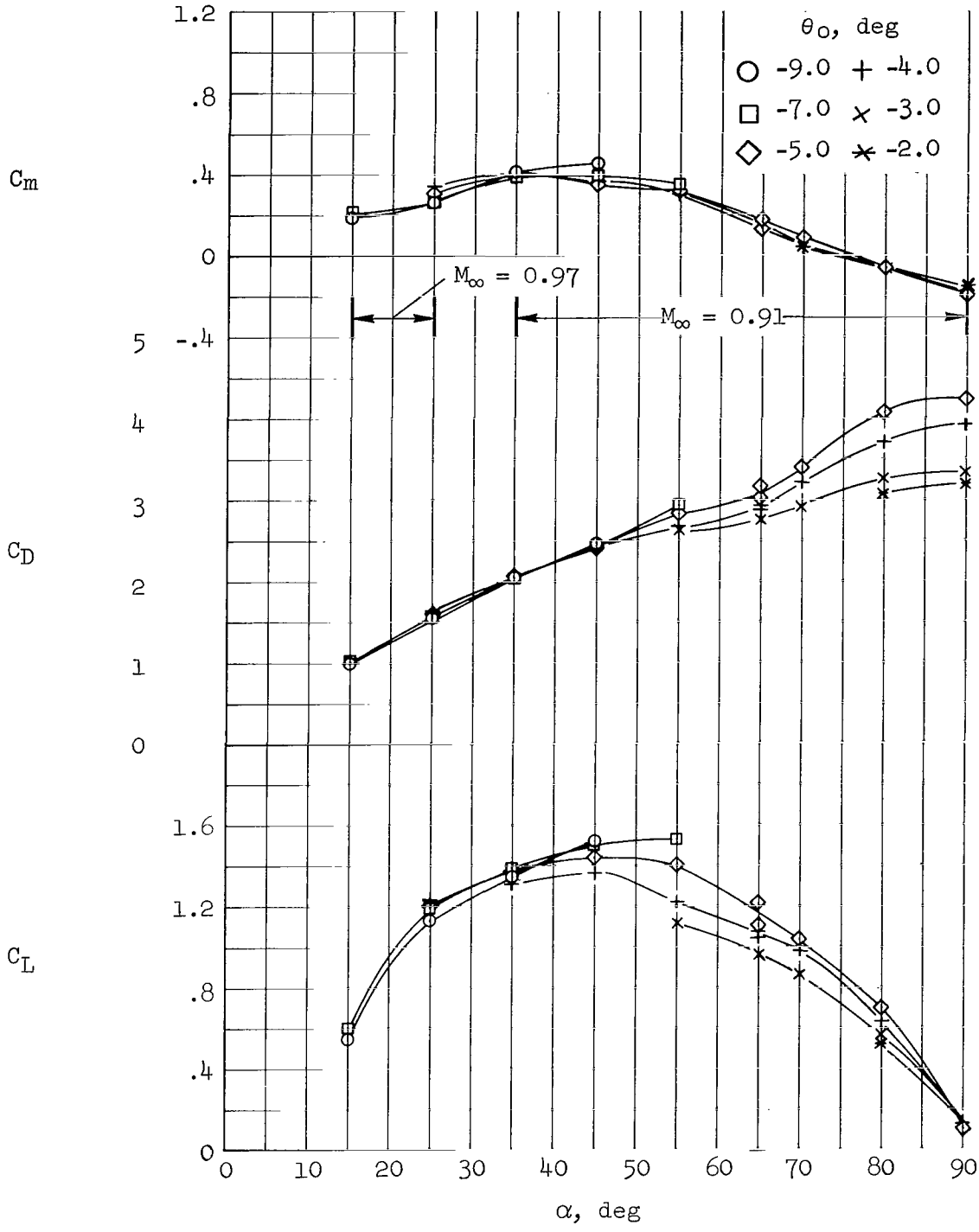

(a) M_∞ = 0.97 and 0.91 as noted

Figure 13.- Aerodynamic characteristics of the body-rotor configuration, short elliptic blades; $\theta_1 = 0^o$, $\theta_2 = 0^o$.

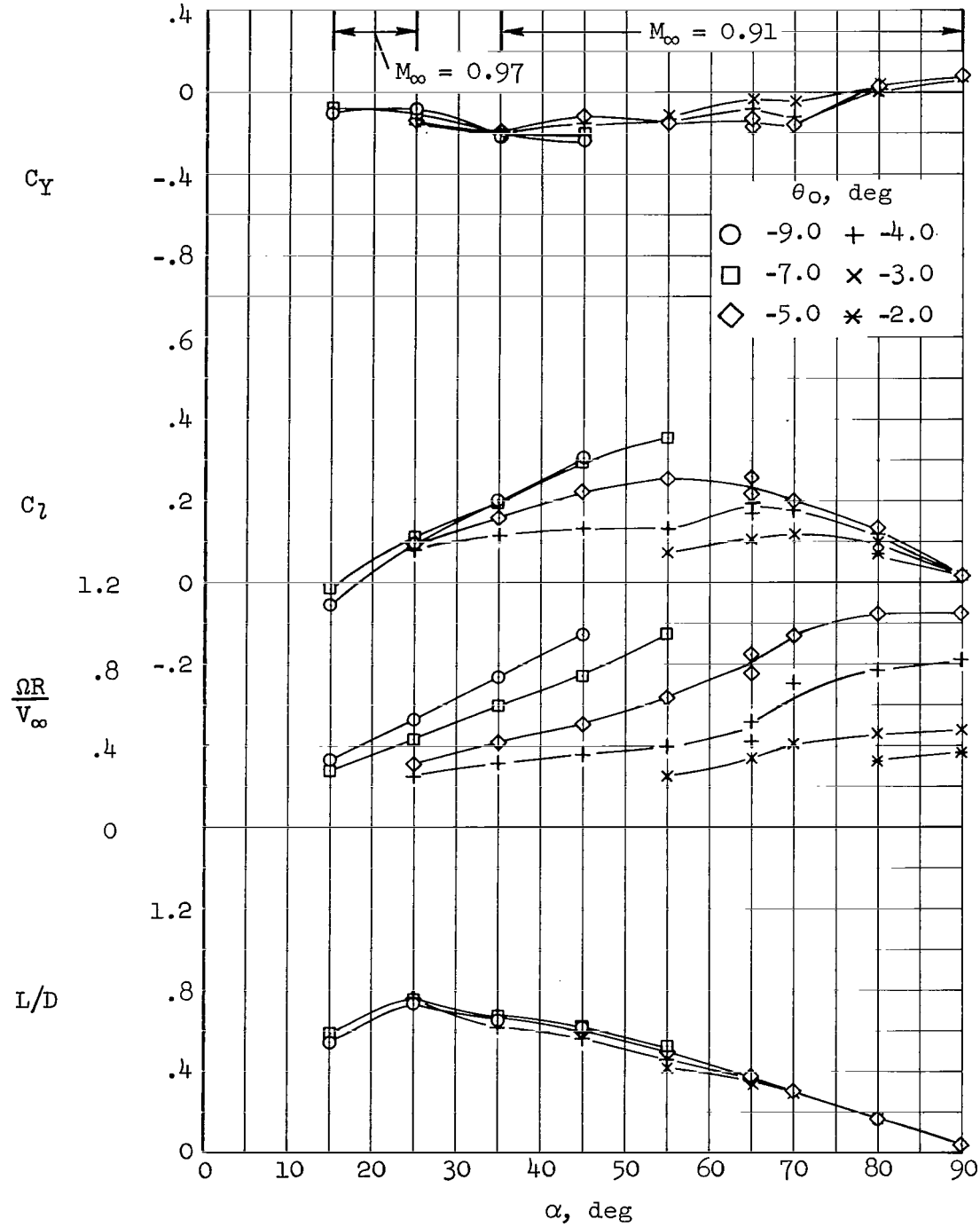

(a) M_∞ = 0.97 and 0.91 as noted - Concluded

Figure 13.- Continued.

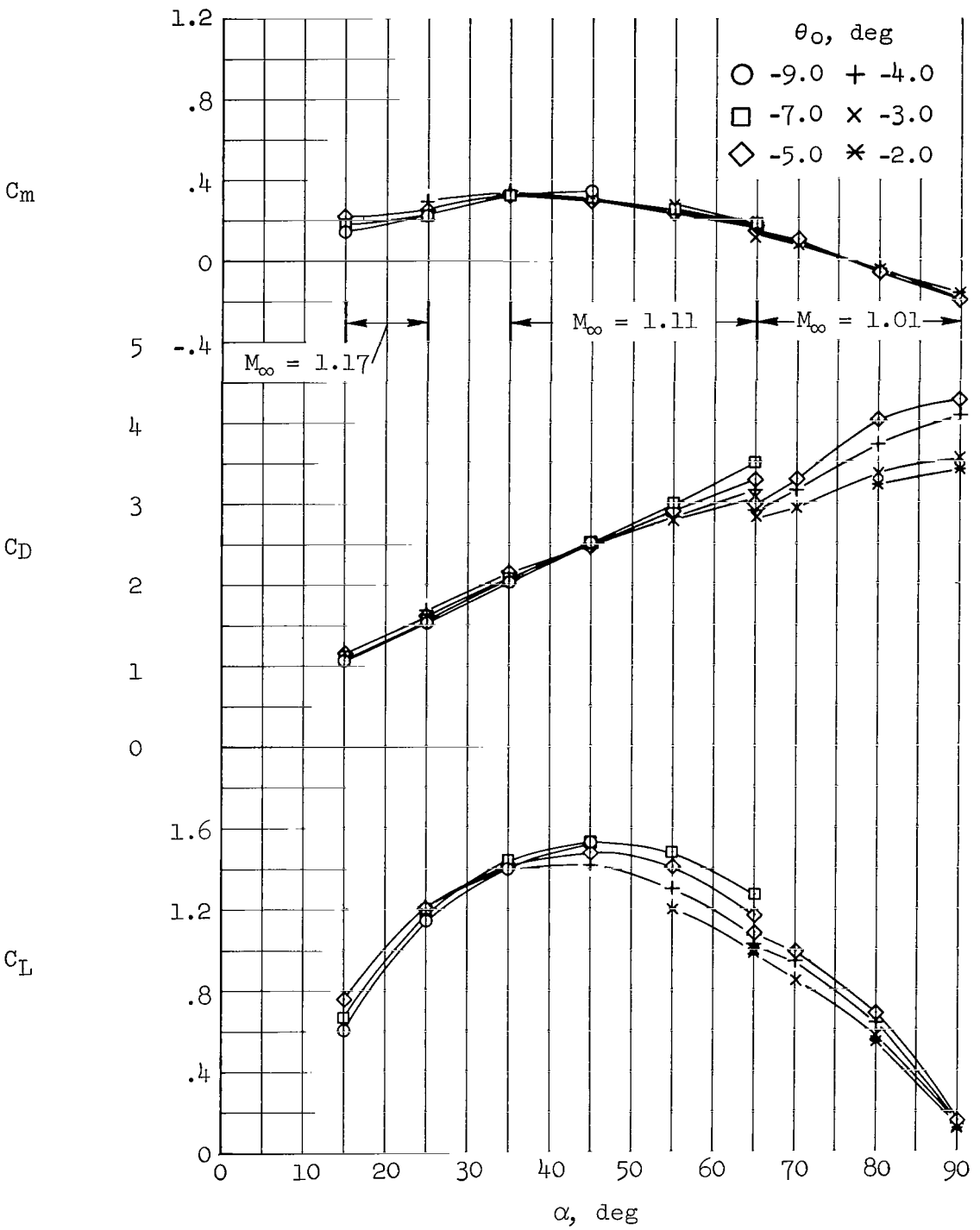

(b) M_∞ = 1.01, 1.11 and 1.17 as noted

Figure 13.- Continued.

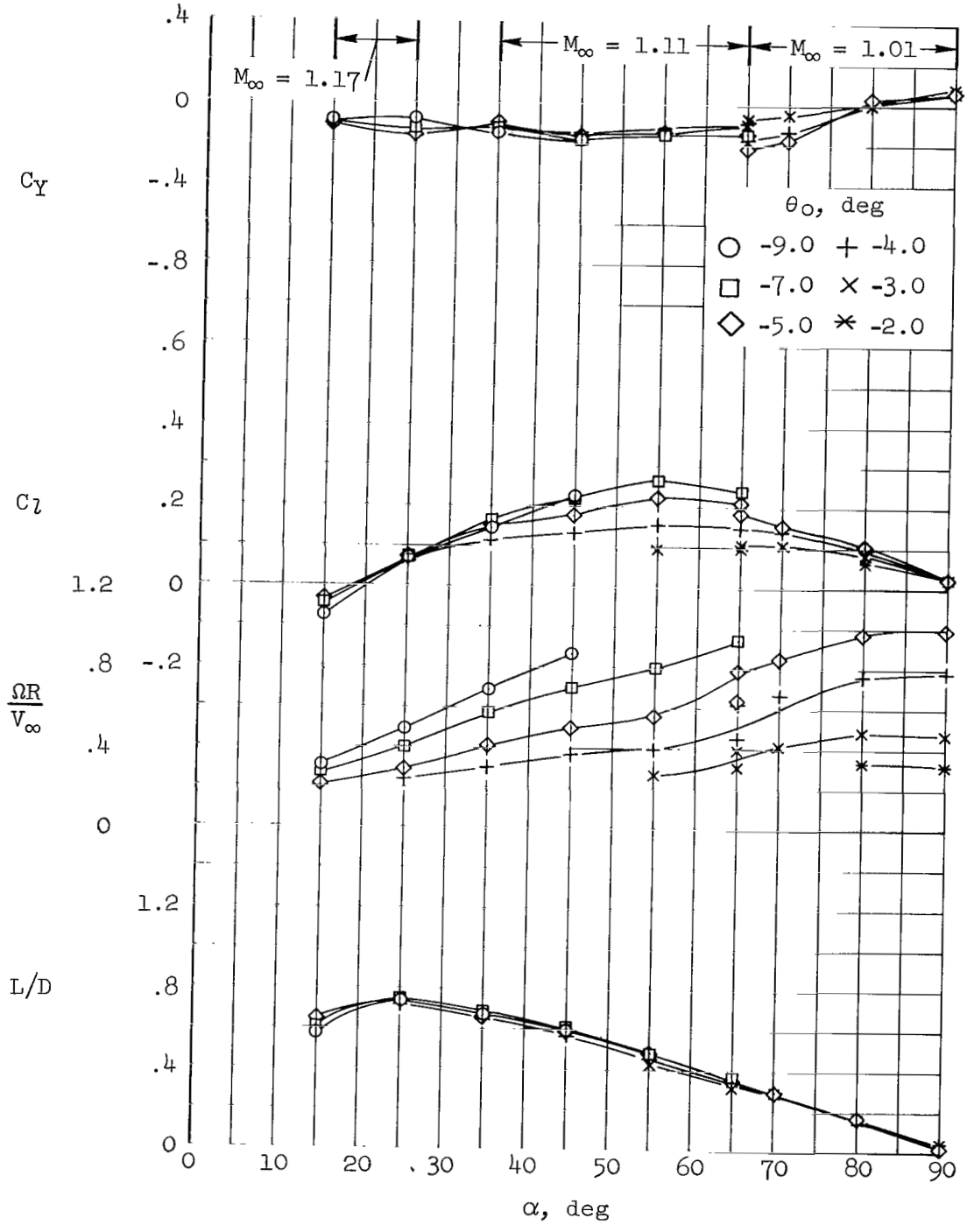

(b) M_∞ = 1.01, 1.11 and 1.17 as noted - Concluded.

Figure 13.- Concluded.

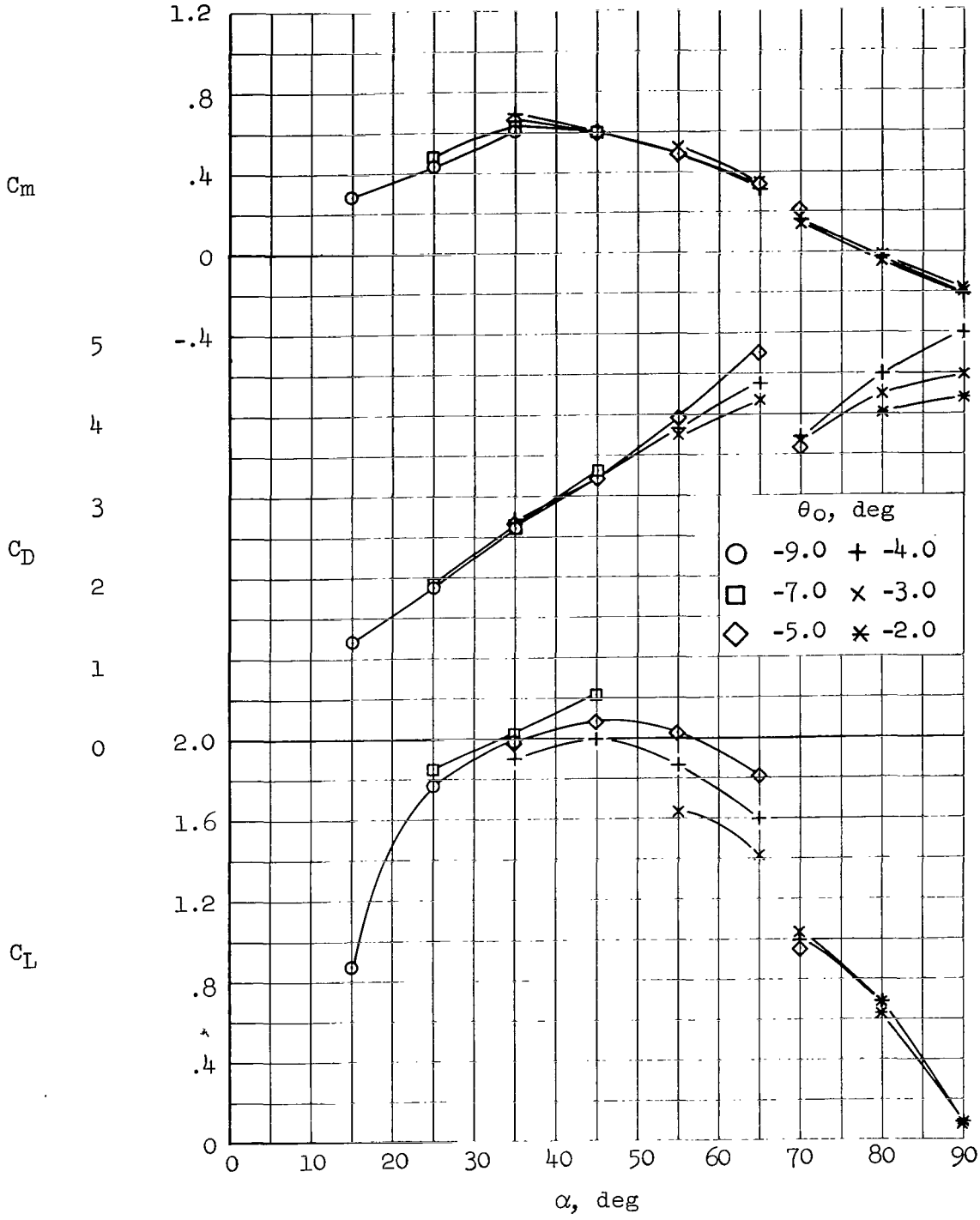

(a) $M_\infty = 0.91$

Figure 14.- Aerodynamic characteristics of the body-rotor configuration, long elliptic blades; $\theta_1 = 0^\circ$, $\theta_2 = 0^\circ$.

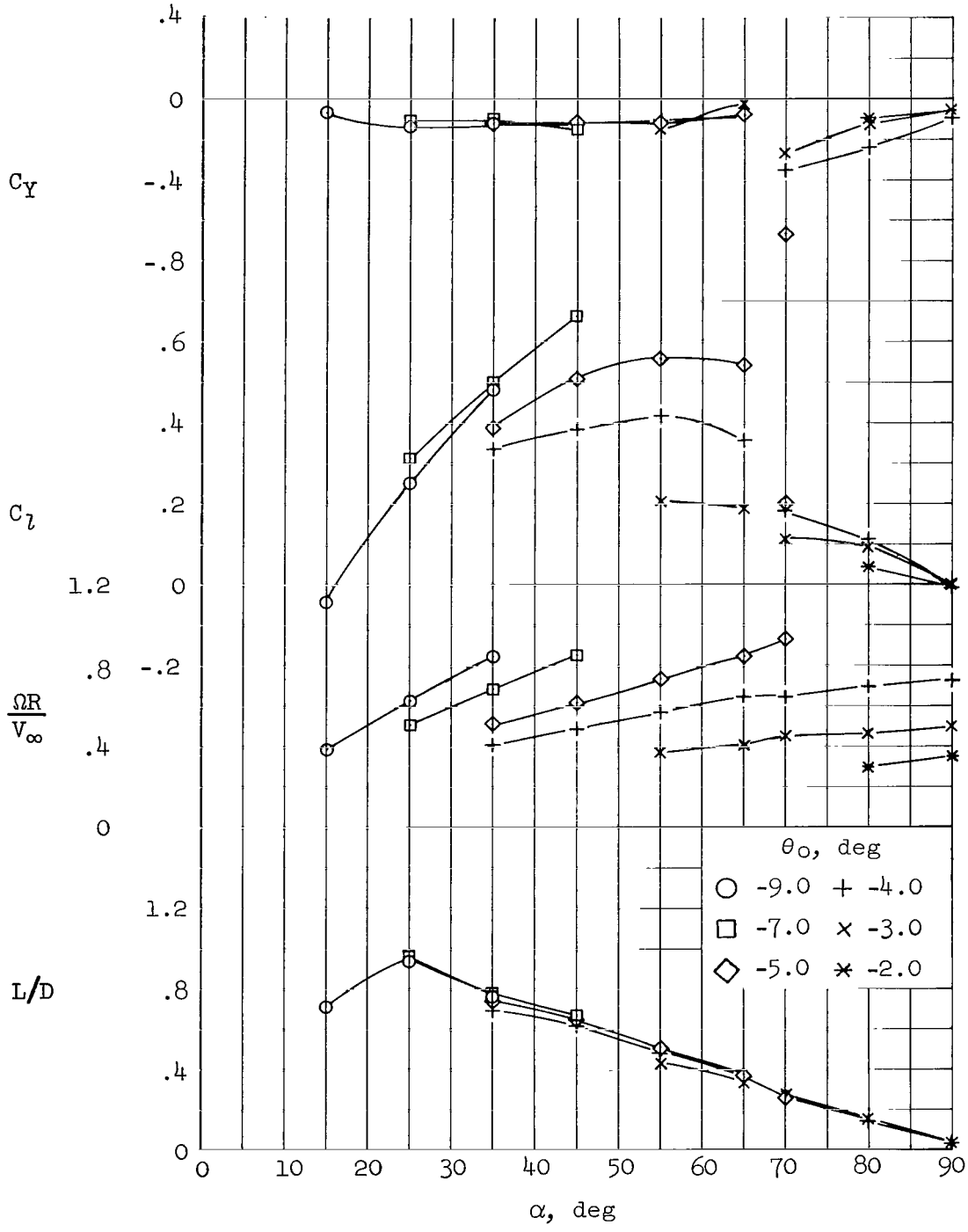

(a) M_∞ = 0.91 - Concluded.

Figure 14.- Continued.

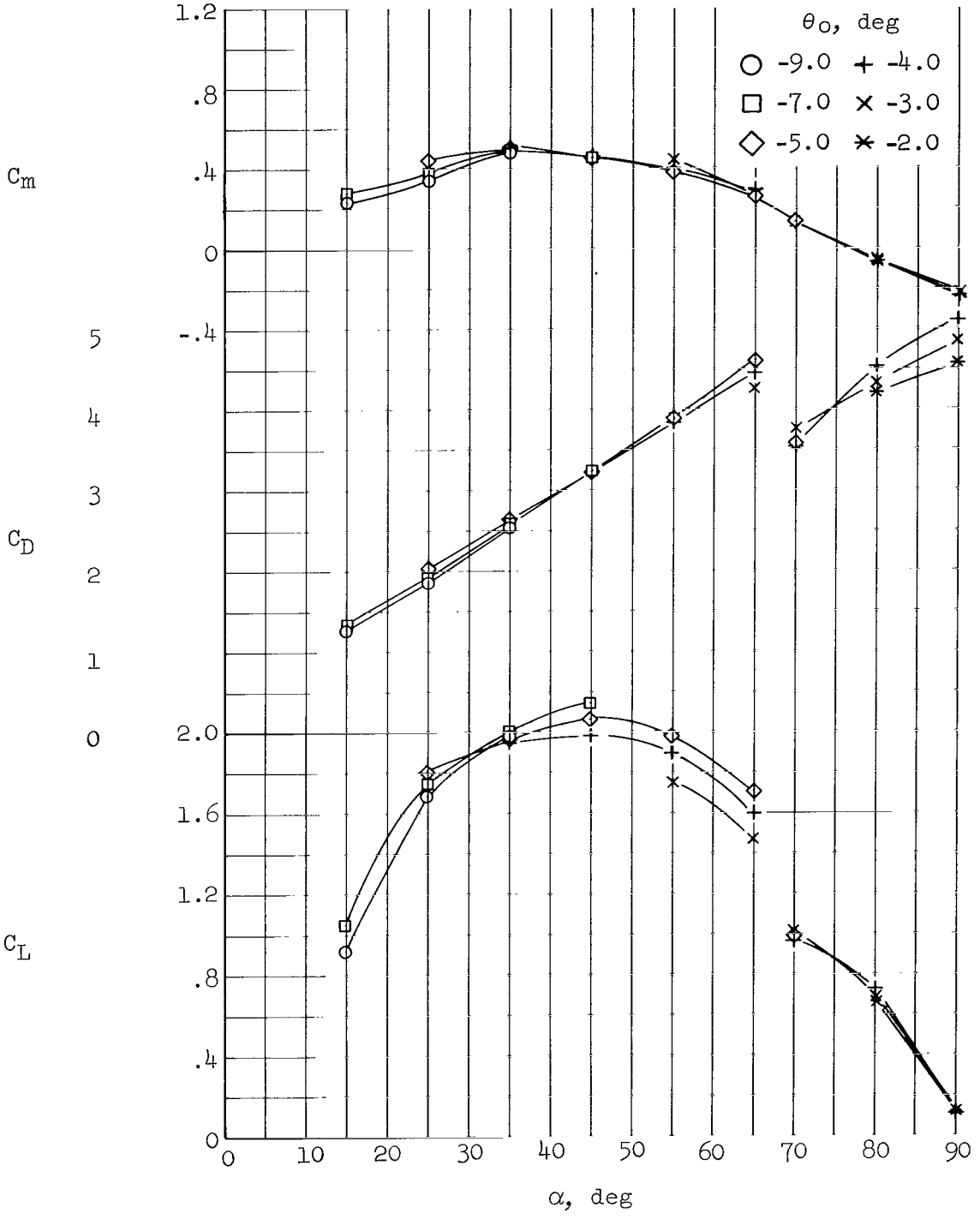

(b) $M_\infty = 1.11$

Figure 14.- Continued.

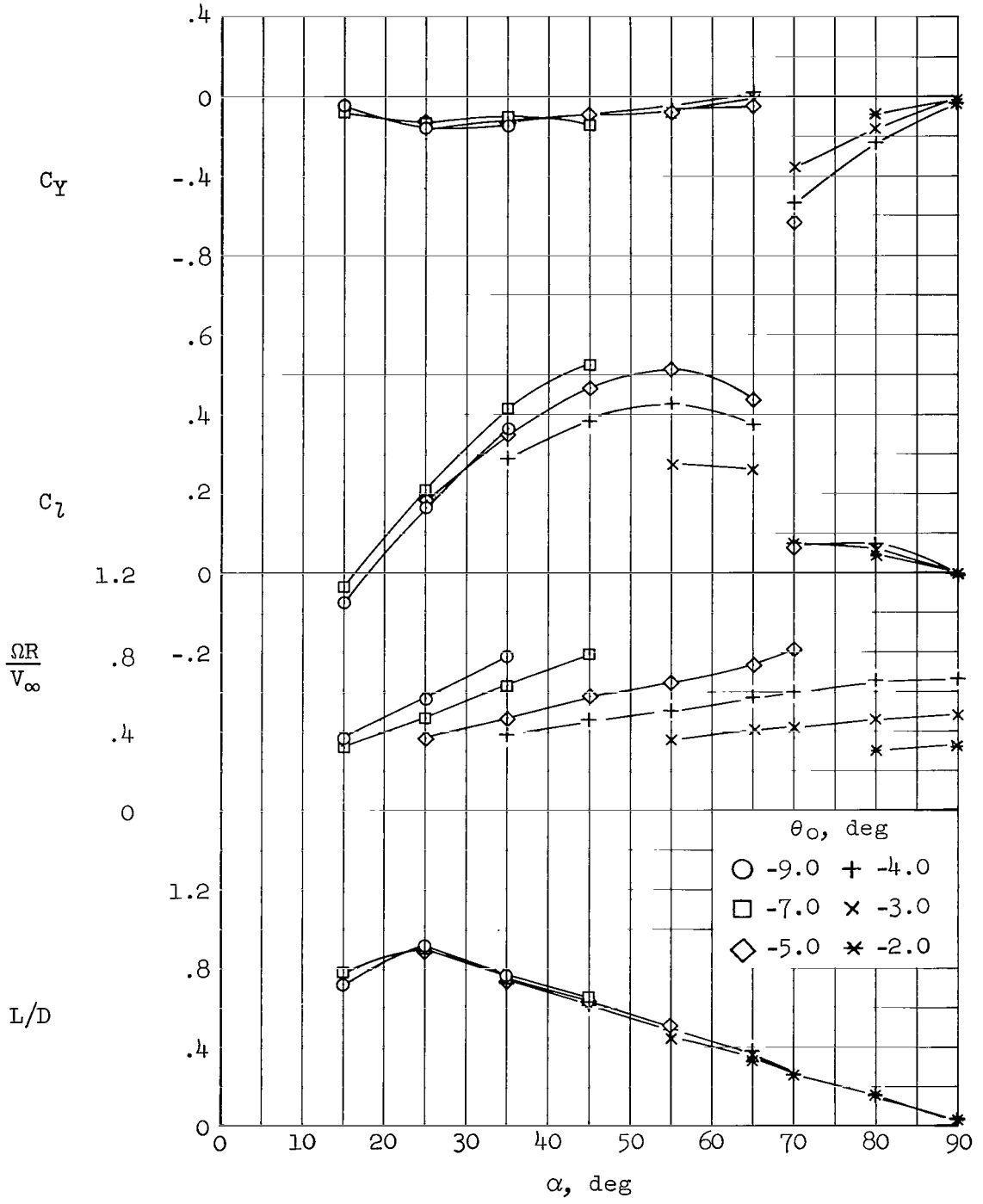

(b) M_∞ = 1.11 - Concluded.

Figure 14.- Concluded.

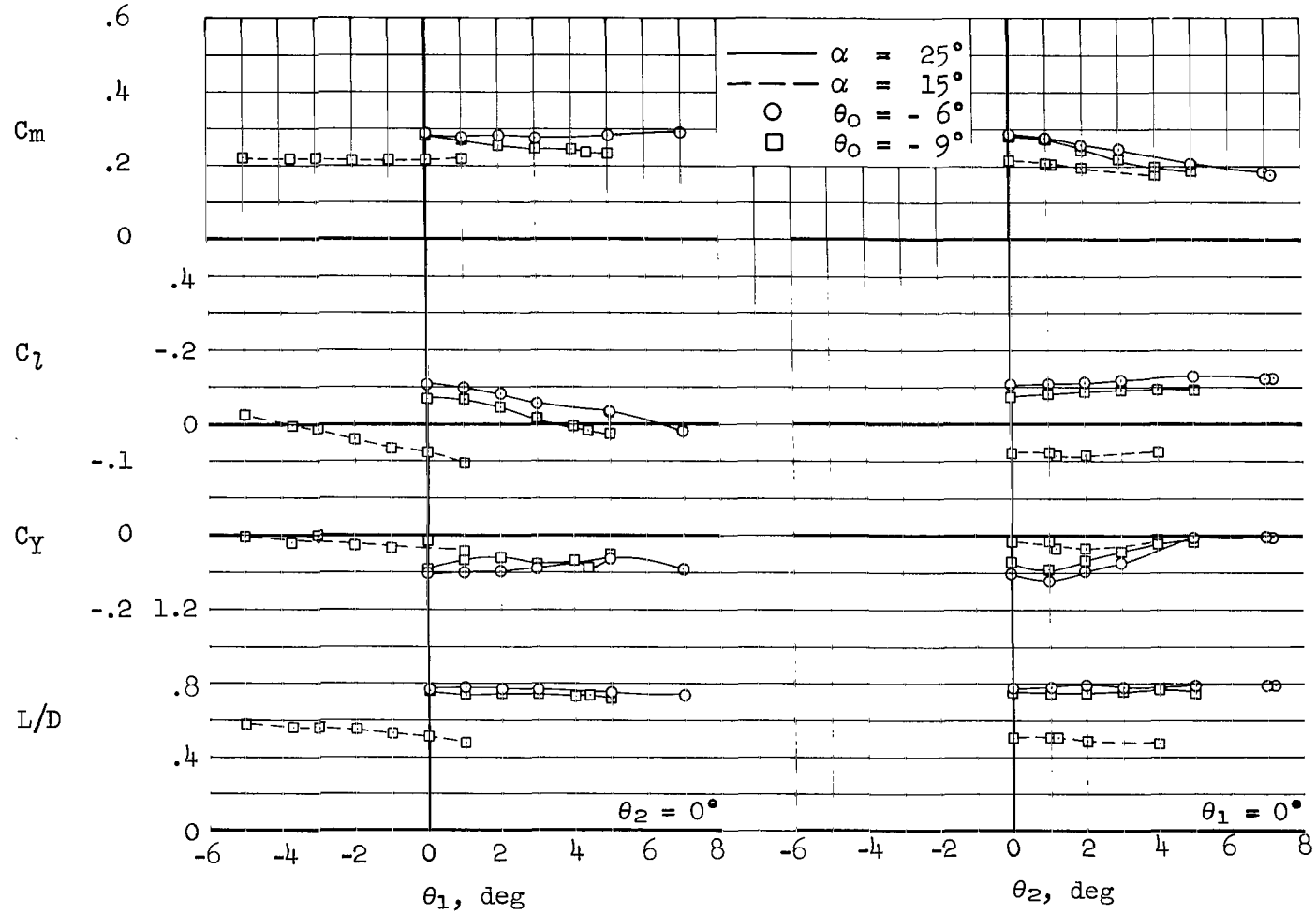

(a) $M_\infty = 0.93$

Figure 15.- Cyclic pitch control characteristics of the body-rotor configuration; double-wedge blades.

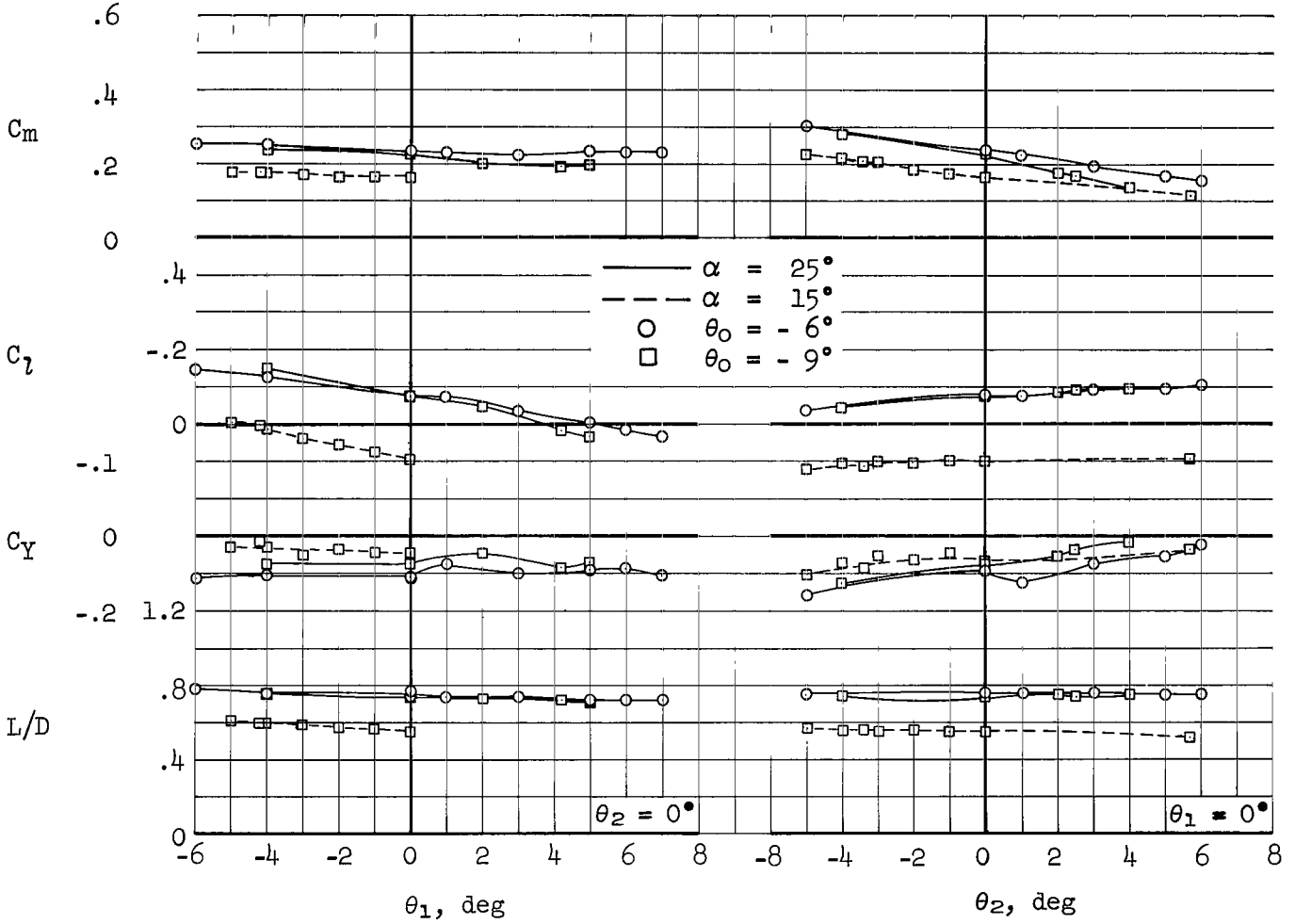

(b) M_∞ = 1.12

Figure 15.- Concluded.

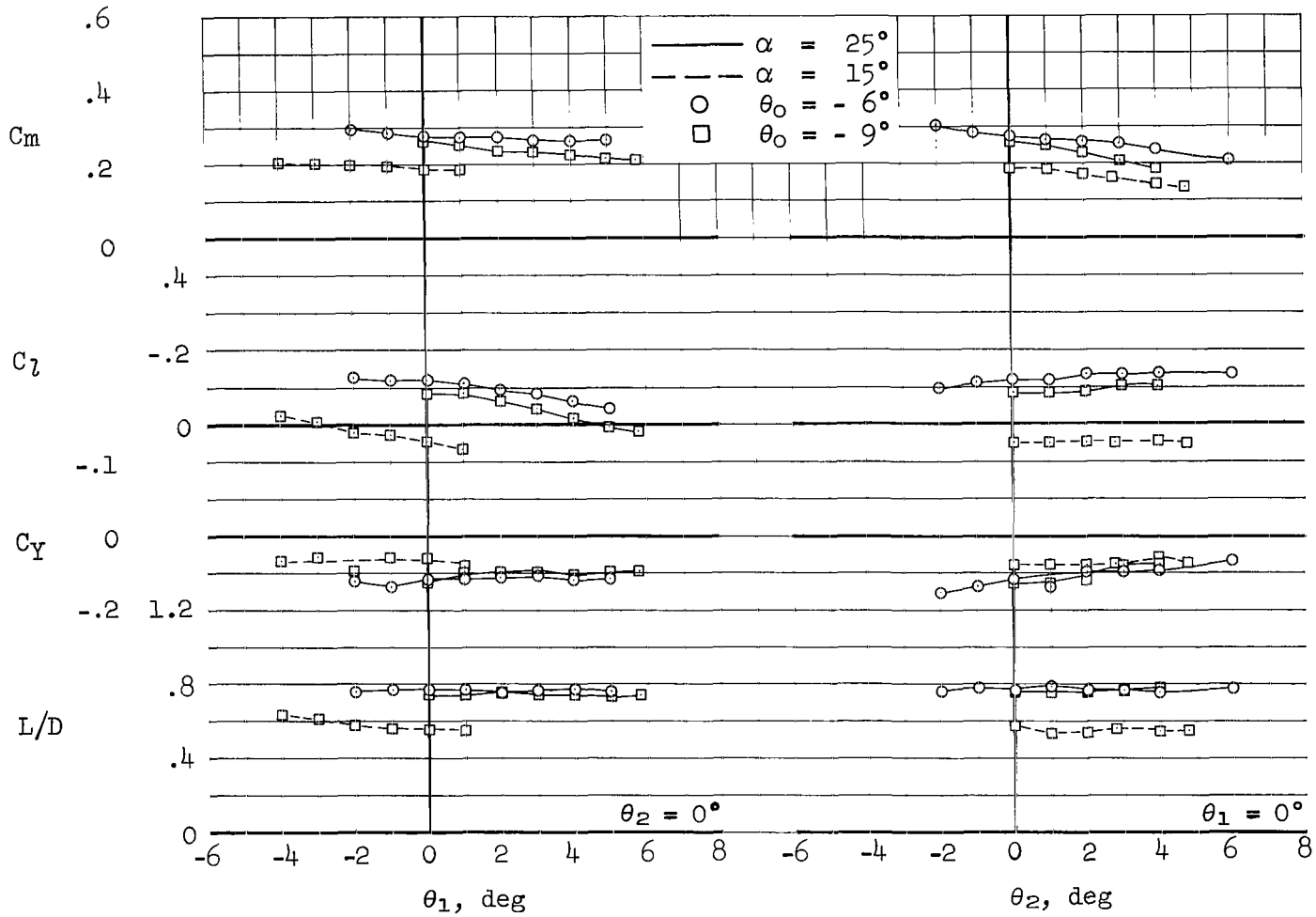

(a) $M_\infty = 0.97$

Figure 16.- Cyclic pitch control characteristics of the body-rotor configuration; short elliptic blades.

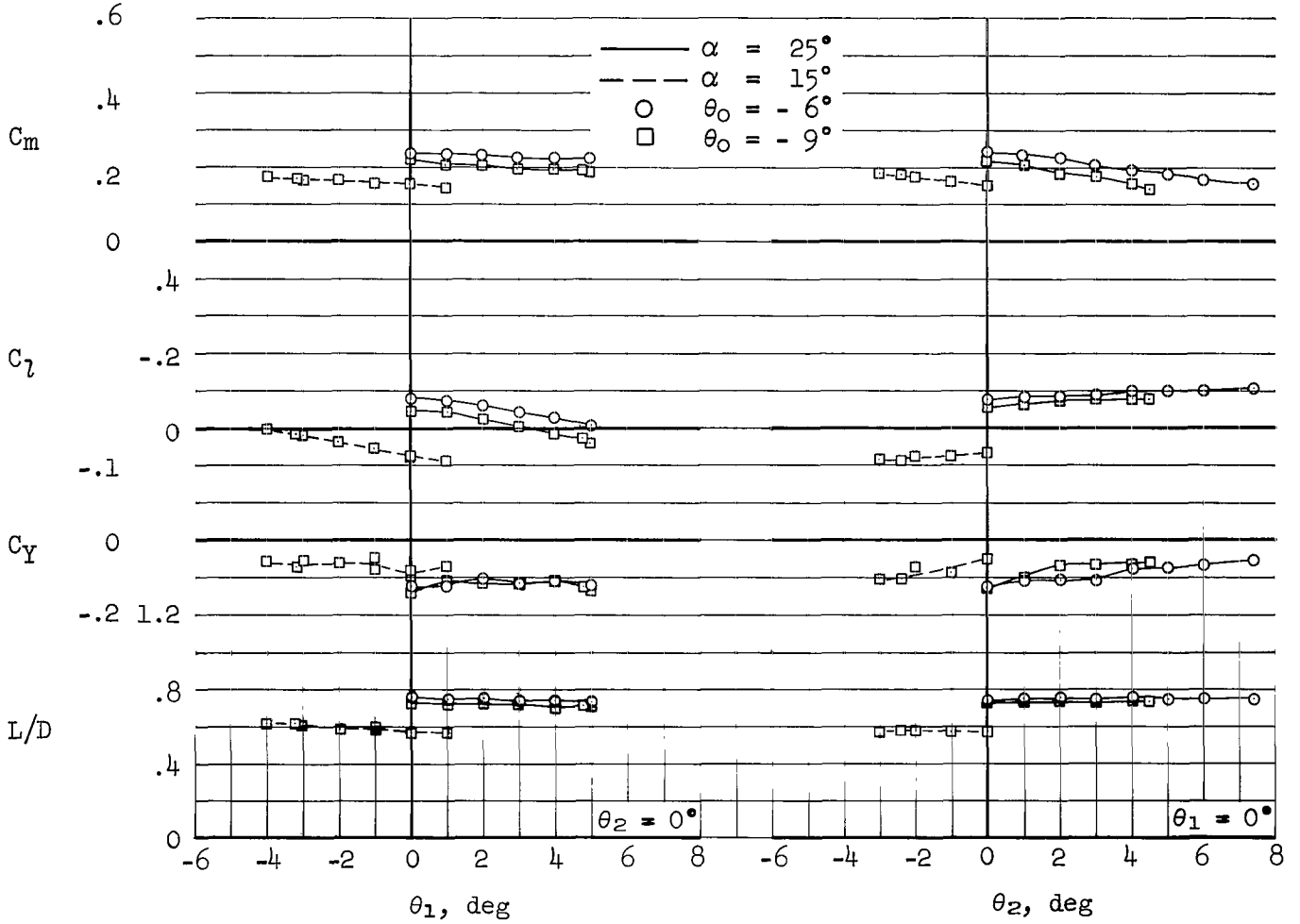

(b) $M_\infty = 1.17$

Figure 16.- Concluded.

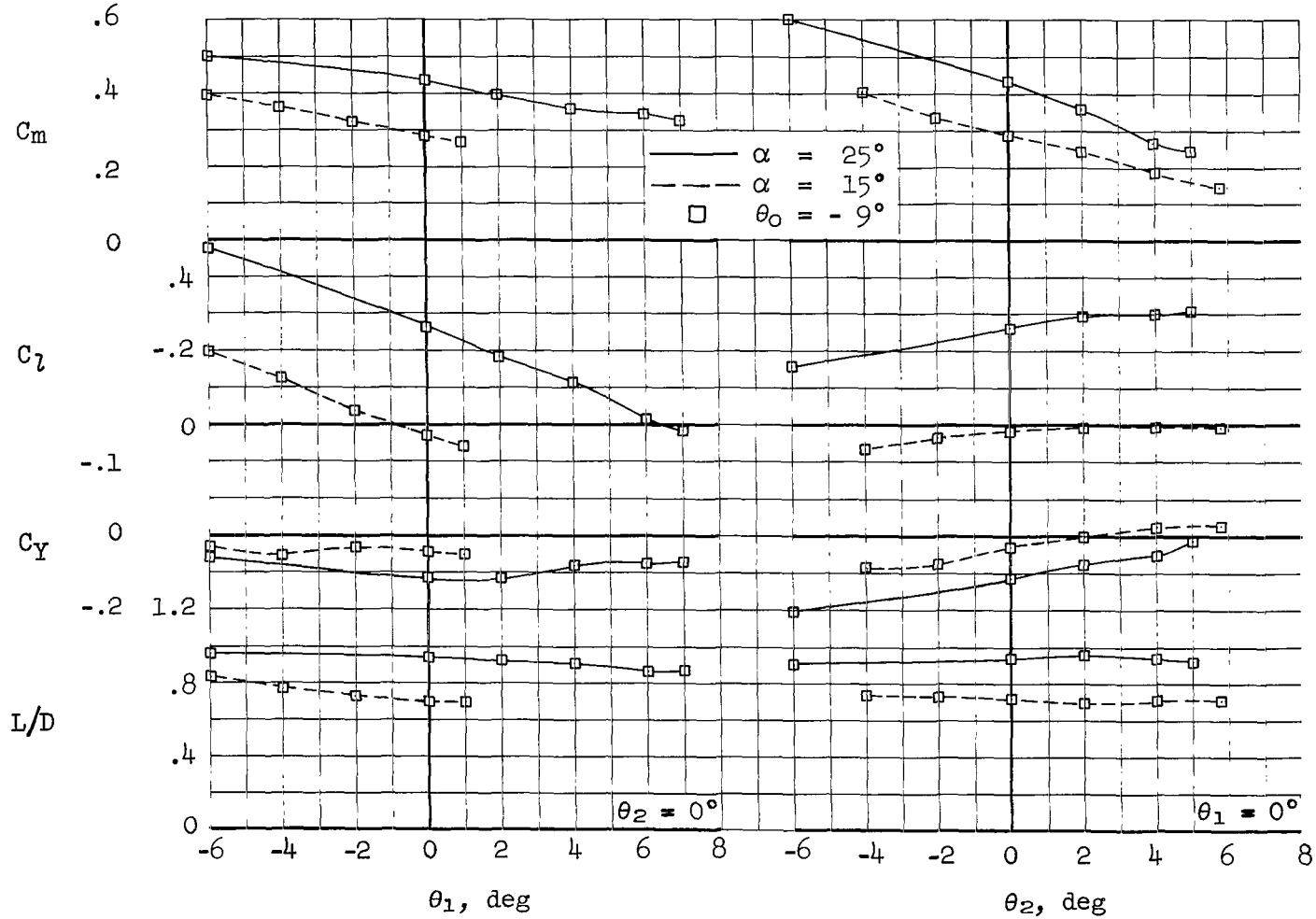

(a) $M_\infty = 0.91$

Figure 17.- Cyclic pitch control characteristics of the body-rotor configuration; long elliptic blades.

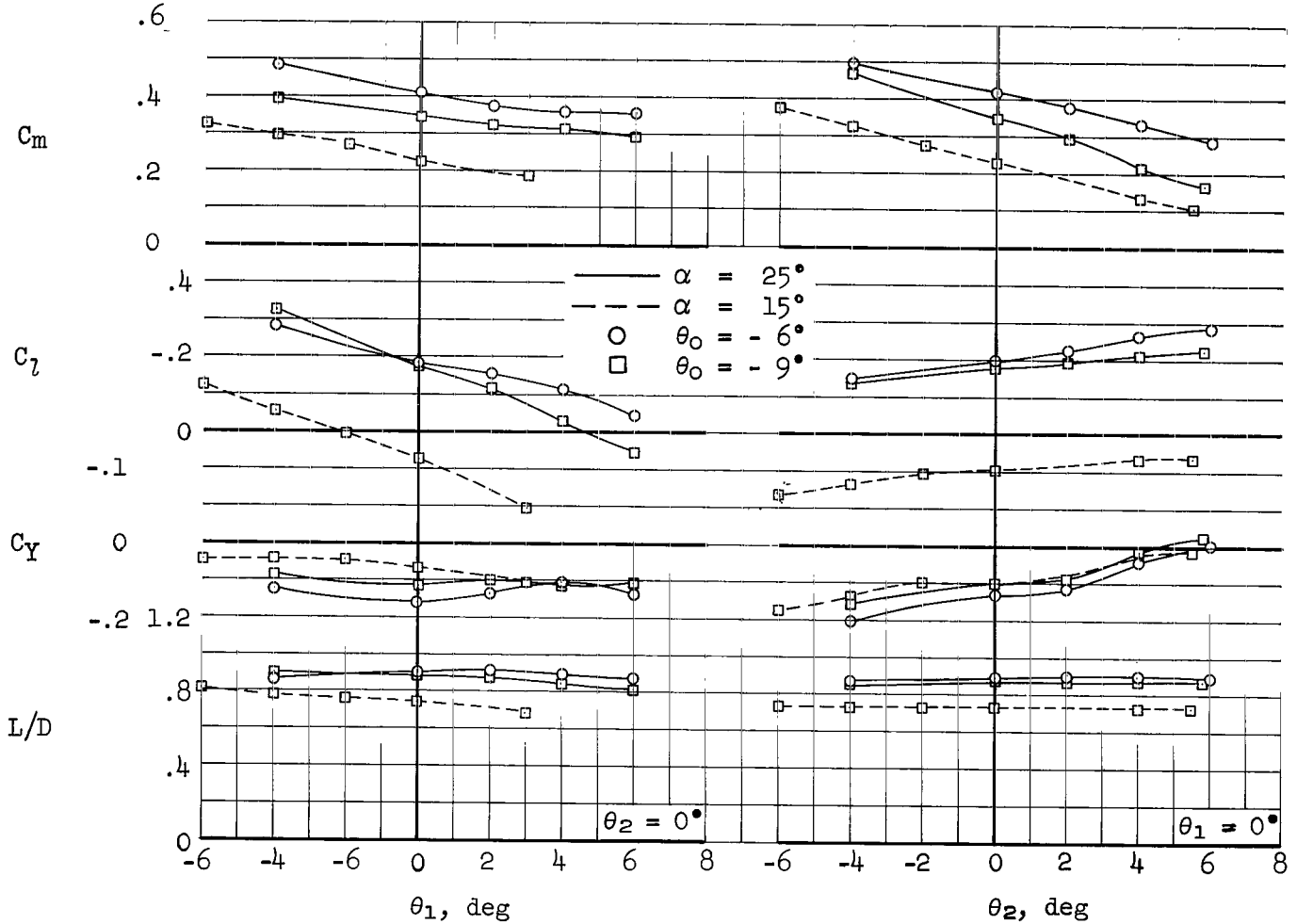

(b) M_∞ = 1.11

Figure 17.- Concluded.

"The aeronautical and space activities of the United States shall be conducted so as to contribute . . . to the expansion of human knowledge of phenomena in the atmosphere and space. The Administration shall provide for the widest practicable and appropriate dissemination of information concerning its activities and the results thereof."

—NATIONAL AERONAUTICS AND SPACE ACT OF 1958

NASA SCIENTIFIC AND TECHNICAL PUBLICATIONS

TECHNICAL REPORTS: Scientific and technical information considered important, complete, and a lasting contribution to existing knowledge.

TECHNICAL NOTES: Information less broad in scope but nevertheless of importance as a contribution to existing knowledge.

TECHNICAL MEMORANDUMS: Information receiving limited distribution because of preliminary data, security classification, or other reasons.

CONTRACTOR REPORTS: Scientific and technical information generated under a NASA contract or grant and considered an important contribution to existing knowledge.

TECHNICAL TRANSLATIONS: Information published in a foreign language considered to merit NASA distribution in English.

SPECIAL PUBLICATIONS: Information derived from or of value to NASA activities. Publications include conference proceedings, monographs, data compilations, handbooks, sourcebooks, and special bibliographies.

TECHNOLOGY UTILIZATION PUBLICATIONS: Information on technology used by NASA that may be of particular interest in commercial and other non-aerospace applications. Publications include Tech Briefs, Technology Utilization Reports and Technology Surveys.

Details on the availability of these publications may be obtained from:

SCIENTIFIC AND TECHNICAL INFORMATION OFFICE

NATIONAL AERONAUTICS AND SPACE ADMINISTRATION

Washington, D.C. 20546